Copyright Warning & Restrictions

The copyright law of the United States (Title 17, United States Code) governs the making of photocopies or other reproductions of copyrighted material.

Under certain conditions specified in the law, libraries and archives are authorized to furnish a photocopy or other reproduction. One of these specified conditions is that the photocopy or reproduction is not to be "used for any purpose other than private study, scholarship, or research." If a, user makes a request for, or later uses, a photocopy or reproduction for purposes in excess of "fair use" that user may be liable for copyright infringement,

This institution reserves the right to refuse to accept a copying order if, in its judgment, fulfillment of the order would involve violation of copyright law.

Please Note: The author retains the copyright while the New Jersey Institute of Technology reserves the right to distribute this thesis or dissertation

Printing note: If you do not wish to print this page, then select "Pages from: first page # to: last page #" on the print dialog screen

ABSTRACT

METHANE PARTIAL OXIDATION OVER PHTHALOCYANINE CATALYST

by
Yuan Zhu

The partial oxidation reaction of methane over a zeolite-supported ruthenium phthalocyanine catalyst is studied in a packed bed reactor. The investigation of such reaction is desirable because partial oxidation of methane yields a synthesis gas that can be upgraded to liquid chemicals and fuels.

Reactants of this study are He-diluted CH_4 and O_2. The effluent includes unreacted CH_4 and O_2, He, CO, CO_2, H_2, and H_2O vapor. Thermal conductivity gas chromatography is applied to identify the mole fractions of reactants and products. System pressure is maintained at 50 psig. Experiments are run at 250, 275, 300, 325, 350, and 375 ℃. For each temperature, the feed molar ratio of CH_4/O_2 is varied from 0.5 to 5.0.

Although reaction temperature is more than 200 ℃ lower than that of common catalytic methane partial oxidation, conversion of methane is obvious. Product analysis indicates that the highest conversion is 80.4% at 375 ℃, CH_4/O_2=0.5. Conversion of methane increases with increasing temperature, but it decreases with increasing molar ratio CH_4/O_2. Selectivities of both H_2 and CO increase with the increasing temperature or molar ratio CH_4/O_2. But selectivity of CO_2 decreases with the increasing temperature or molar ratio CH_4/O_2.

Based on a differential packed bed reactor model, the global rate of CH_4 reaction shows first order dependencies on each of O_2 and CH_4. The overall reaction rate is a second-order reaction. The reaction rate constant k for each temperature was also

determined. An Arrhenius plot of the global rate constants suggest that the reaction is limited by reaction kinetics between 250-300 ℃, and limited by mass transfer between 300-375 ℃. Equilibrium calculations are also made for all cases in this study. The result shows that products selectivities of equilibrium calculation are significantly different from that of catalytic reactions, which emphasizes the effective catalytic actions of the zeolite-supported ruthenium phthalocyanine.

METHANE PARTIAL OXIDATION OVER PHTHALOCYANINE CATALYST

by
Yuan Zhu

A Thesis
Submitted to the Faculty of
New Jersey Institute of Technology
in Partial Fulfillment of the Requirements for the Degree of
Master of Science in Chemical Engineering

Otto H. York Department of
Chemical, Biological and Pharmaceutical Engineering

May 2013

APPROVAL PAGE

METHANE PARTIAL OXIDATION
OVER PHTHALOCYANINE CATALYST

Yuan Zhu

Dr. Robert Barat, Thesis Advisor — Date
Professor of Chemical, Biological and Pharmaceutical Engineering, NJIT

Dr. Edward Dreyzin, Committee Member — Date
Professor of Chemical, Biological and Pharmaceutical Engineering, NJIT

Dr. Xianqin Wang, Committee Member — Date
Assistant Professor of Chemical, Biological and Pharmaceutical Engineering, NJIT

BIOGRAPHICAL SKETCH

Author: Yuan Zhu

Degree: Master

Date: May 2013

Undergraduate and Graduate Education:

- Master of Science in Chemical Engineering,
  New Jersey Institute of Technology, Newark, NJ, 2013

- Bachelor of Science in Chemical Engineering,
  China University of Petroleum, P. R. China, 2010

Major: Chemical Engineering

谨以此硕士论文，献给我亲爱的的父亲、母亲

To my beloved parents, for their love, support, and encouragement

ACKNOWLEDGMENT

I would like to show my great heartfelt appreciation to Prof. Robert B. Barat, who not only served as my research supervisor, providing valuable resources and amazing academic guidance, and showing me the superb research methods, guidance, but also building up my confidence by his trust and encouragement. I am also fully grateful to his care on my daily life. It is my huge honor to get acquainted and serve with such an brilliant grandmaster.

Special gratitude to Prof. Edward L. Dreyzin and Prof. Xianqin Wang for serving as my committee member and their brilliant advises.

I also appreciate Dr. Larisa Krishtopa and Dr. Jeong Seop Shim of the NJIT Materials Characterization Lab for their help.

This research is cooperated with Chemistry Department of Seton Hall University. Also I wish to thank Prof. Sergiu M. Gorun and his group for their support and contribution.

Their concerning, love, support, selfless, encouragement and sacrifice made me keep moving forward. ― Finally, I give my most sincere gratitude to my beloved parents.

TABLE OF CONTENTS

TABLE OF CONTENTS
(Continued)

TABLE OF CONTENTS
(Continued)

Chapter **Page**

TABLE OF CONTENTS
(Continued)

Chapter **Page**

LIST OF TABLES

LIST OF FIGURES

LIST OF FIGURES
(Continued)

Figure **Page**

LIST OF FIGURES
(Continued)

Figure **Page**

CHAPTER 1

INTRODUCTION

1.1 The Necessity of Methane Processing

Methane (CH_4) is the main component of natural gas, landfill gas and a by-product from oil refining and chemical processing. It has enormous potential value as a source of clean fossil energy or as a raw material provided it can be brought to the point of use economically. [1] As crude oil reserves decrease and advanced natural gas exploration techniques are applied, new gas reservoirs such as shale gas fields, natural gas and shale gas will become increasingly important in the energy and chemical supplies of the future. [2] Natural gas reservoirs are large and widespread throughout the world, mainly in the Middle East and Russia, although other areas, including the United States, also have their fair share. The estimated reserves at the end of 2006 to amounted approximately 6300 trillion cubic feet. [1]

If there is no economical local market for natural gas, it needs to be either liquefied for transport, or chemically converted on-site into useful fuels or chemicals for eventual transport to market. Though easy to do, flaring - burning without any heat recovery - of the natural gas is wasteful. It also contributes greenhouse gases to the atmosphere without any useful return. Liquefying natural gas consumes much energy, and losses occur while transporting and storing. There are also storage and shipment safety issues with liquefied natural gas.

1.2 Possible Conversion Pathways for Methane

Since methane makes up as much as 92% of natural gas, on-site chemical conversion must focus on the chemistry of methane. Figure 1.1 shows the two main routes of methane chemical conversion: Direct and indirect. Direct conversion includes oxidative coupling of methane to ethylene, oxidation of methane to methanol or formaldehyde, etc. Indirect conversion means converting methane into synthesis gas (syngas – a mixture of primarily CO and H_2) first, then conversion of the syngas to liquid fuels by Fischer–Tropsch process, or to methanol. The other is liquid fuel (methanol is most important), which could be used to replace petroleum products (such as gasoline). [3] Nowadays, many countries are adding methanol, mainly converted from natural gas, into gasoline, which has been proved positive. Moreover, syngas could be used to synthetize fine chemicals or ammonia

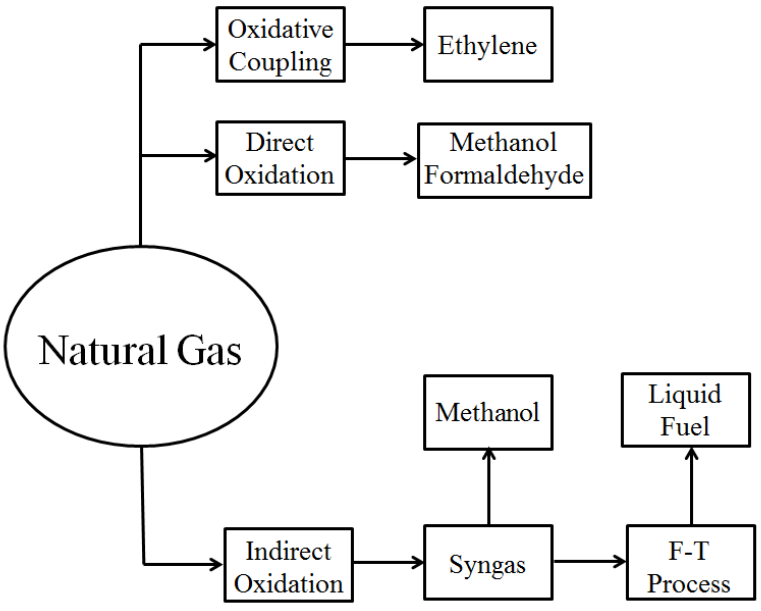

Figure 1.1 Main routes of methane conversion.

1.2.1 Direct Conversion of Methane

Direct conversion means converting natural gas into chemical products without passing through intermediates. A typical example is direct partial oxidation of methane to methanol or formaldehyde. This processing route, of great interest, is considered to have great potential for industrialization. Oxygen (O_2) and hydrogen peroxide (H_2O_2) are available oxidants for this process. But serious disadvantages of this route exist. Since methane is a very stable molecule, its reactions have generally high activation energies. Once activated, it is difficult to keep the conversion within pre-determined limits.

Because the desired methanol and formaldehyde products are much easier to be oxidized than methane, the selectivity of direct methane conversion to methanol and formaldehyde is unsatisfying. The products are more likely to be oxidized deeply into CO and CO_2. Conceptually, direct methods should have a distinct economic advantage over indirect methods, but to date no direct processes have reached a commercial stage. Desired product yields are generally smaller when operating in a single-pass mode (less than 5%), which makes separations difficult and costly. [2, 3]

An alternative route of direct conversion is oxidative coupling of methane (OCM). The oxidative coupling of methane involves the reaction of CH_4 and O_2 over a catalyst at high temperatures to form C_2H_6 as a primary product and C_2H_4 as a secondary product. [2] Since the pioneering work of Keller and Bhasin in 1982, there has been intensive research on the topic of OCM. [4] Due to an inherent limit, however, the yield of C_2 product achieved in a packed-bed catalytic reactor is only about 25%. This is because of complete oxidation reactions occurring in the gas phase and partially on the catalyst surface, which lowers substantially the C_2 selectivity especially under the conditions of high temperature

and pressure. So far only a selectivity of up to 70% has been achieved with more than 30% methane conversion. Moreover, due to the low concentration of ethylene in the exit stream, the cost of its separation is high. [4, 5, 6] Therefore, although much research is done on OCM, this technology still has not yet been commercialized.

1.2.2 Indirect Conversion of Methane

In indirect routes, methane is first converted to an intermediate, most commonly to synthesis gas (syngas). The syngas is subsequently converted to the desired product(s) by a related downstream catalytic conversion. At present, most commercialized natural gas conversions are based on indirect routes.

Currently, two viable large-scale approaches for converting methane to liquid hydrocarbons are in use: the methanol-to- gasoline (MTG) route, and Fischer–Tropsch (FT) synthesis. [1] Syngas, produceded from natural gas, is raw material of FT synthesis. Fischer–Tropsch synthesis typically begins with upgrading the hydrogen (H_2) content by a catalytic water-gas shift reaction. The FT process then catalytically hydrogenates carbon monoxide (CO) into predominantly straight aliphatic hydrocarbon chains. [6] The catalytic synthesis of methanol also uses syngas as feedstock.

Both processes begin with the production of syngas from methane. Conversion of methane to syngas by an oxidant is an important step in indirect conversions of methane. The most common oxidants include water (Steam reforming), CO_2 (Dry reforming), and O_2 (Partial oxidation). [6] Steam reforming is currently widely applied in industry. However, it requires high temperatures, usually above 600 ◦C, with corresponding high energy consumption. [1] Thus, there is considerable of room for research and development. Lowering reaction temperature and energy consumption is preferred. The partial oxidation

of methane to synthesis gas offers this chance.

1.3 Catalytic Partial Oxidation

Methane steam reforming is currently the dominant technology for synthesis gas production. The process is highly endothermic, and industrial production requires large and capital intensive operations. Catalytic partial oxidation of methane is an attractive alternative, since it is slightly exothermic and considerably faster [7]. Moreover, partial oxidation of methane could be operated at high space velocity, and the volume of reactor required is smaller, which significantly lowers the investment of equipment and also production costs. [3]

The ideal global reaction of methane partial oxidation to syngas is:

$$CH_4+0.5O_2 \leftrightarrow CO+2H_2,\ \Delta H_{298k}^{\ominus} = -35.7\text{kJ/mol} \quad (1.1)$$

As it is an exothermic reaction, the partial oxidation process could reduce energy consumption, compared with other technologies. The practical reaction process, however, is more complicated. Side reactions always occurs with the main reaction, including: [3]

Complete oxidation reaction (combustion reaction):

$$CH_4+2O_2 \leftrightarrow CO_2+2H_2O,\ \Delta H_{298k}^{\ominus} = -802\text{kJ/mol} \quad (1.2)$$

Steam reforming reaction:

$$CH_4+H_2O \leftrightarrow CO+3H_2,\ \Delta H_{298k}^{\ominus} = 206\text{kJ/mol} \quad (1.3)$$

CO_2 reforming reaction:

$$CH_4+CO_2 \leftrightarrow 2CO+2H_2,\ \Delta H_{298k}^{\ominus} = 247\text{kJ/mol} \quad (1.4)$$

CO-H_2O (water-gas shift) reaction:

$$CO+H_2O \leftrightarrow CO_2+H_2,\ \Delta H_{298k}^{\ominus} = -41.2\text{kJ/mol} \quad (1.5)$$

Carbon deposition reaction and carbon consumption reaction:

$$CH_4 \leftrightarrow 2H_2 + C,\ \Delta H_{298k}^{\ominus} = 74.9 J/mol \quad (1.6)$$

$$2CO \leftrightarrow C + CO_2,\ \Delta H_{298k}^{\ominus} = -172.4 kJ/mol \quad (1.7)$$

$$CO + H_2 \leftrightarrow C + H_2O,\ \Delta H_{298k}^{\ominus} = -175.3 kJ/mol \quad (1.8)$$

Table 1.1 shows the equilibrium constant for methane partial oxidation to CO and H_2 at different temperatures. The equilibrium constant decreases with the increasing of temperature. But in actual production, due to the equilibrium constant is very favorable, the rate of methane partial oxidation will significantly increase at higher reaction temperatures.

Table 1.1 Equilibrium Constant $\left(K_P = \frac{p_{CO} p_{H_2}^2}{p_{CH_4} p_{O_2}^{0.5}}\right)$ of $CH_4 + 0.5O_2 \leftrightarrow CO + 2H_2$

Temperature/ ℃	K_P
600	2.196×10^{12}
700	1.030×10^{12}
800	6.048×10^{11}
900	4.108×10^{11}
1000	3.056×10^{11}
1200	1.955×10^{11}
1400	1.424×10^{11}
1600	1.028×10^{12}

Source: [3]

1.4 Catalyst for Partial Oxidation

Catalyst development is the core of the research on methane partial oxidation. It is desirable to achieve high CH_4 conversions together with high selectivities to CO and H_2 at lower temperatures. According to their active components, the catalysts could fall into two types. The first type is noble metal catalyst. Noble metals could be directly used as catalysts. As it is precious, however, a noble metal is usually processed into a supported catalyst. Some commonly used noble metals are Rh, Ru, Pd, Pt Ir, etc. The second group consists of supported base metal catalysts, including Ni, Co, Fe, etc. In addition, some transition metal oxide or rare-earth metal oxide supported catalysts have shown a significant catalysis effect on methane partial oxidation.

The catalysts research continues. A desirable partial oxidation catalyst could activate the methane molecule without subsequent of deep oxidation of it to CO_2 and H_2O. [3]

1.4.1 Noble Metal Catalyst

Horn, etc. [8] showed that methane could convert into syngas, where H_2/CO=2/1, on Rh and Pt foam catalysts. Selectivity of this reaction is very high. Kunimori, etc. [9, 10] found that $RhVO_4/SiO_2$ and Rh/SiO_2 are all excellent catalysts for partial oxidation, with 90% conversion of methane achieved at 700 ℃. The $RhVO_4/SiO_2$ could make the reaction occur at 500 ℃. The initiation temperature of Rh/SiO_2 is above 600 ℃. Schimidt, etc. [11] compared activities of monolith-supported Rh, Pt, Ir, Pd, Pd-La_2O_3 and Ni, Fe, Co, Re catalysts. The best conversion of methane, 89%, was achieved on Ru at 1000 ℃. Activity of Ni was close to Ru, but deactivation occurred. Pd, Pd-La_2O_3, and Co deactivated rapidly, while Re and Fe showed no catalytic activity. Furthermore, they also tested Rh, Pt, and Ni

supported by α-Al_2O_3. Methane conversion was over 90% on Rh and Ni, and selectivity was over 95%. Activation of Pt was lower than Rh and Ni.

Noble catalysts have such advantages: high activity, good stability, and strong carbon deposit resistance. Ru and Pt are the best on activity and stability among all of them. However, the cost of applying noble metal catalysts industrially is high, which can limit their development.

1.4.2 Base Metal Catalyst

Because of considerable activity, good stability and lower cost, Fe, Co and Ni catalysts were widely studied. Among this series of metal, Ni has the best activation, which is close to Pt.

Choudhary, etc. [12, 13] researched activation on NiO catalyst supported by MgO, CaO, Al_2O_3, SiO_2 and rare earth oxides. The result indicated that when supported by CaO, the catalyst could maintain a high efficiency for long times with no carbon deposit. After making Co addition onto NiO/Yb_2O_3, NiO/ZrO_2, and NiO/ThO_2, the initiation temperature was lowered, and deposited carbon was also decreased. Dissanayake, etc. [14] studied partial oxidation reaction over 25wt% Ni/Al_2O_3 within 450-900 ℃.They found that CH_4 was almost completely converted when temperature was over 700 ℃. And selectivity of CO was beyond 95%.

Table 1.2 shows the commonly used noble metals and base metals catalysts. Although noble catalysts have excellent properties such as high activity, good stability, and strong carbon deposit resistance, they are costly. Ni-based supported catalyst for partial oxidation of methane to syngas has similar activation with Ru and other noble metals. The much lower cost of Ni-based catalysts led to much research. But the disadvantages of

Ni-based catalyst are also obvious. The catalyst loses its activity due to sintering and depositing carbon. Therefore, solutions for these problems are the key of practical application.

Table 1.2 Noble Metals and Base Metals with Supports in Common Use

Noble Metal	Support	Base Metal	Support
Rh	Al_2O_3, Monolith m-Sm_2O_3, c-Sm_2O_3 M_2O_3 (M=Sc, Y, La, Al)	Co	La_2O_3, γ-Al_2O_3
Pd	MO_2 (M=Ti, Zr, Hf, Ce), Eu_2O_3	Mn, Fe, Cu	La_2O_3
Ir	Al_2O_3, Monolith	Ni	CaO, Monolith $NiAl_2O_4$, ZrO_2
Pt	Ln_2O_3, Al_2O_3, TiO_2 (Ln=Pr, Sm, Eu, Gd, Tb, Dy, Tm, Yb, Lu)	Re	Al_2O_3, Yb_2O_3, MgO

Source: [3]

1.5 Metal Phthalocyanine

A phthalocyanine is an intensely blue-green colored aromatic macrocyclic compound widely used in dyes. Phthalocyanines are structurally related to other macrocyclic pigments, especially the porphyrins. Both feature four pyrrole-like subunits linked to form a 16-membered ring. [15]

Phthalocyanine forms coordination complexes with most elements of the periodic table, such as shown in Figure 1.2. These complexes are also intensely colored and also are used as dyes or pigments. [15] The simplest phthalocyanine is abbreviated as $H_{16}Pc$. The number 16 refers to the H atoms on the outermost rings. The Pc is shorthand for phthalocyanine. A Ru-coordinated phthalocyanine shown in Figure 1.2, and is written as $H_{16}PcCu$. In a substituted Pc, some or all of the outermost H atoms are replaced by other atoms (e.g. Fluorines) or groups (e.g. alkyl).

1.5.1 Property and Structure

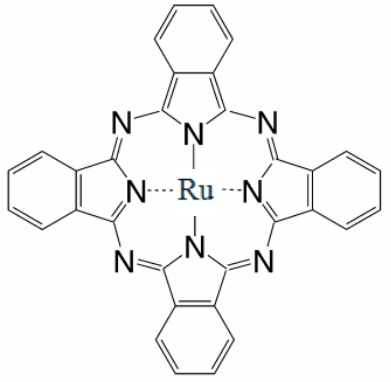

Figure 1.2 . Molecular structure of $H_{16}PcRu$.

Source: [18]

Unsubstituted phthalocyanine ($H_{16}Pc$), and many of its complexes have limited solubilities in organic solvents. Benzene at 40 ℃ dissolves less than a milligram of $H_{16}Pc$ or $H_{16}PcRu$ per liter. They dissolve easily in sulfuric acid due to the protonation of the nitrogen atoms bridging the pyrrole rings. Many phthalocyanine compounds are thermally very stable. They do not melt but can sublime; for example, $H_{16}PcCu$ sublimes at >500 ℃ under inert gases (nitrogen, CO_2). Substituted phthalocyanine complexes often have much higher solubility. They are less thermally stable and often cannot be sublimed. Unsubstituted phthalocyanines strongly absorb light between 600 and 700 nm, thus these materials are blue or green. Substitution can shift the absorption towards longer wavelengths, changing the color from pure blue to green to colorless (when the absorption is in the near infrared).

1.5.2 Application as Oxidation Catalyst

Due to the special structure and properties of metal phthalocyanines, research has been done on their catalytic performance. Ruthenium Pc complexes have been investigated in a range of catalytic applications. [16] Although a significant amount of research investigating metal phthalocyanines as catalysts has focused on cobalt and iron derivatives, ruthenium phthalocyanine complexes show a similar level of catalytic versatility in many cases such as reduction catalyst, hydrogenation catalyst, cyclopropanation catalyst and oxidation catalyst.

In the research by Chan and Wilson, Jr. [17] zeolite-encased PcRu showed activity in the partial oxidation of methane in a fixed-bed flow reactor. Reaction conditions were 375 ℃, 50psig, CH_4/O_2=4, gas hourly space velocity (GHSV) =2600h^{-1}. Methane conversion was only 4.8%. Selectivities of CO_2, H_2O and CH_3OH were 87%, 1%, and

11.3%, respectively. The highest conversion of methane (18.2%) was achieved over PcFe with 1.2% selectivity of H_2 under same reaction conditions, but there was no CH_3OH generated. At higher temperatures methane conversions were generally increased, but methanol yields significantly decreased. This result suggested that PcRu decomposed at high temperature and therefore deactivated. The characteristic blue green color and purple color disappeared after the high temperature reactions. Comparing with other metals (Co, Fe) tested in this research, PcRu was the only catalyst that showed activity and it contained less metal complex than others. [17]

1.6 Objectives

In this study, Ru-coordinated phthalocyanine catalyst anchored to zeolite was produced by partners (S. Gorun group) at the Chemistry Department, Seton Hall University. This research includes running experiments of methane partial oxidation over the PcRu catalyst, data collection and analyses, reactor modeling and comparison to experimental data, and proposing a possible reaction mechanism.

In experiments, both mass of catalyst and reaction pressure are fixed. Some appropriate temperatures are selected for experiments. For every temperature, two groups of experiments need to be done. In the first group, the total flow rate of reactants was fixed, while the feed ratio of CH_4/O_2 is varied. In the second part, while trying to keep the ratio of CH_4/O_2 constant, the total flow rate is varied.

On-line gas chromatography/thermal conductivity detection GC/TCD will be used to detect and measure gas species. From peak areas, mole fractions of reactants, and most products could be worked out. Methane conversion is determined for every experimental run, as are carbon balances. Reactor outlet concentrations are also compared with calculated equilibrium concentrations.

An appropriate reactor model is selected. According to species balance and reaction conditions, the reactor model is evaluated using collected methane conversion data. Global reaction orders and rate constants for each temperature are estimated. An Arrhenius plot is used to suggest potential mass transfer limitations. Finally, the observed model will be used to PREDICT methane conversions of selected experiments from a separate database. This comparison will test the strength of the global model.

CHAPTER 2

EXPERIMENTAL APPARATUS AND PROCEDURE

2.1 Experimental Apparatus

A block diagram of the entire experimental system is shown in Figure 2.1. The apparatus consists of mass flow control and delivery; a stainless steel tubular packed bed reactor (PBR); an electric furnace; and an on-line sampling and analysis. The analyzing instrument is a thermal conductivity detector gas chromatograph (GC/TCD).

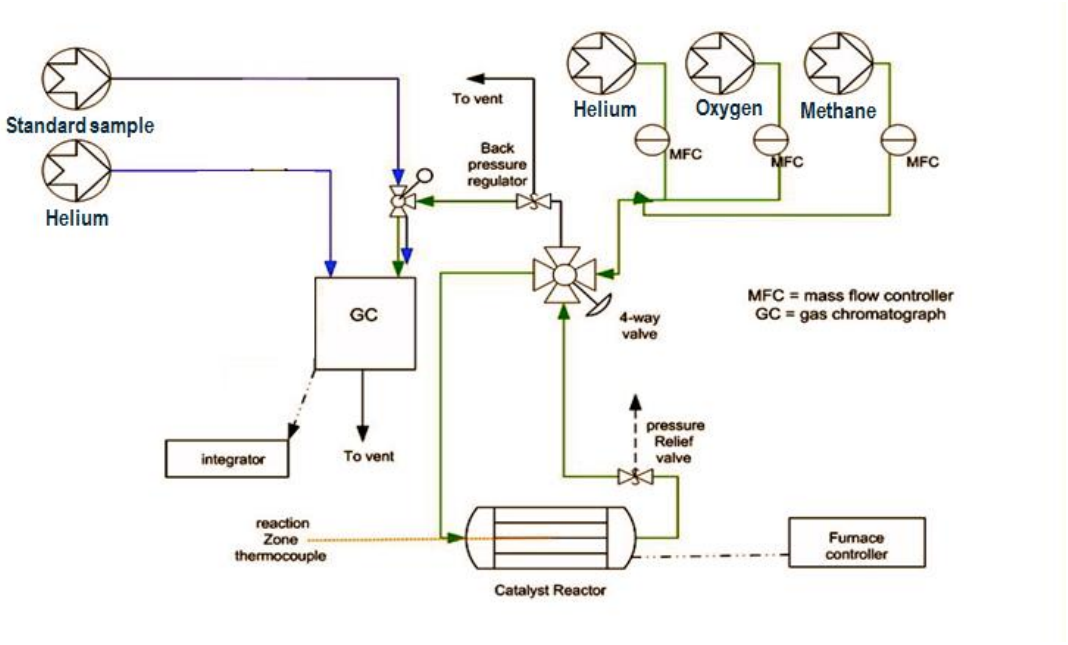

Figure 2.1 Experimental system block diagram.

2.1.1 Gas Flow

The flow rate of reactants (CH_4, O_2) and diluent (He) are well maintained by calibrated mass flow controllers. Gases for the GC are also controlled by mass flow controllers. The pressure in the flow system is maintained by a back-pressure regulator. A 4-way valve

allows the operator to direct either feed gas (reactor bypass) or reactor effluent for on-line sampling for GC/TCD analysis.

2.1.2 Reactor

The packed bed reactor (PBR) is prepared with a (1/2 inch OD) stainless steel tube. The tube rests in a 3-zone, temperature-controlled electric furnace. Axially-inserted thermocouples measure the temperature just upstream and just downstream of the PBR zone inside this tube. Excellent isothermal conditions are easily obtained in this study.

The phthalocyanine catalyst (H_{16}PcRu) supported by zeolite is a fine powder, which was synthesized by Prof. Gorun's group from the Chemistry Department of Seton Hall University, and provided to NJIT under subcontract. The powder was directly plugged into the tube and well fixed by glass wool in the two sides at first. But the pressure drop was so big that gas flow could not pass through the reactor. To avoid such a problem, the powdered catalyst was pressed into pellets by using a tablet machine. Then pellets were broken into 2-3 mm chunks by using a small chopper. The catalyst in chunks was fixed in the tube by glass wool in the two ends. This wool+chunk zone constitutes the PBR.

2.1.3 Gas Analysis

A model 5890 Hewlett-Packard gas chromatograph with TCD is used. Helium is used as carrier flow gas for the CG/TCD. For all experiments, carrier flow rate is 30 standard cubic centimeters per minute (sccm). The GC He source regulated pressure is 80 psig. The GC oven temperature is kept at 30 ℃, attenuation at 0, and range at 3. The peaks are recorded by and quantified on a laboratory PC using the Vernier Logger-Pro software.

Two gas standards were used. The first contains CO (1%, mole fraction, similarly hereinafter), CO_2 (1%), O_2 (1.01%), and CH_4 (1%), with balance He; the second contains H_2 (7%) and N_2 (93%). In the calibration experiments, standard sample is delivered on-line into the GC/TCD. As mole fractions of all components are all known, we could get the fraction-area function for every component (except water vapor) is obtained. Regulated pressures of the two standard cylinders are both 27 psig. A gas sample valve is used for injecting a known amount of gas, collected into a sample loop, into the GC/TCD. This sample loop is always filled to the SAME pressure and at the same temperature for both calibration and experimental samples. This ensures consistent chromatographic analysis.

2.2 Summary of Typical Experimental Steps Followed

Before running experiments, make sure all gas sources are sufficient. During the partial oxidation experiments, make sure that He is fed at first, then O_2 and CH_4. When heating up the furnace, to protect the catalyst, feed He only through the reactor.

Raise the reactor temperature to the point desired. Switch the 4-way valve to make O_2, CH_4 and He to bypass the reactor. Sample the feed for GC/TCD analysis. Then, redirect the feed through the reactor. Wait several minutes till the effluent flushes the whole post-reactor piping, then sample for the GC/TCD. Peak areas of products and unreacted reactants will also be converted into mole fractions.

2.3 Safety Consideration

In order to keep the reaction pressure constant, a pressure relief valve and a back pressure regulator are applied. The regulator is set for a reaction pressure at 50 psig. For safety

consideration, relief gas and all effluent are discharged to vent. Any leak of the system will lead to inaccurate experimental result, or even safety risks in lab. Therefore, seal test must be done for the whole system before any experiment. Inspection should be focused on connections of tubes or flow meters, where leaks likely exist.

2.4 Chemical System Studied

Reactants O_2, CH_4 and Helium are fed from compressed gas cylinders, whose outlet pressure are all 70 psig. Another Helium cylinder is needed as carrier gas for the GC/TCD, with the outlet pressure at 80psig.

Chan and Wilson, Jr. [17] observed methane conversion at 375℃, 50psig, CH_4/O_2=4, gas hourly space velocity (GHSV) =2600h^{-1}, with selecting He as diluent for reactants and carrier gas for GC. Therefore, similar reaction conditions and the same use of He are selected for current research to be consistent with their work. Chan and Wilson, Jr. also indicated that their catalyst likely deactivated when heating over 400℃. Thus, experimental temperature range is set to be 250-375℃, set the range of CH_4/O_2 to be 0.5-5.0. Total flow rate is 645 sccm, flow rate of Helium is 590 sccm. System pressure is 50psig. The mass of catalyst is 9.91gram.

CHAPTER 3

DATA ANALYSIS

3.1 Experimental Gas Composition

For each workday, a GC/TCD calibration test is done as the first experiment. Subsequent analysis of mole fractions is based on the result of this calibration experiment. Table 3.1 lists typical sample data of a calibration test. In all cases (up to 7% for H_2), the TCD response (peak area) is linear with gas concentration.

Table 3.1 Sample Data of Calibration Experiment

Species	Composition (x) (mole %)	Retention time (s)	Peak area (y) (mV ·s)	Calibration Relations
O_2	1.01	~171	149.1	y=147.6x
CO	1	~180	155.0	y=155x
CH_4	1	~320	132.4	y=132.4x
CO_2	1	~790	186.9	y=186.9x
H_2	7	~121	0.9595	y=0.1371x

The compositions (x) in Table 3.1 are already known, since they are based on calibrated mixtures obtained from gas vendors (Scott Gas).The measured GC/TCD peak areas, are taken as y. The GC/TCD is known to be linear over a wide range; so a one-point calibration is sufficient. The only exception is H_2. The calibration for H_2 is limited to a maximum of 7% due to a non-linear response beyond that level. This is due to H_2 having a higher thermal conductivity than the He carrier gas. All the other gas species in this study

have lower values than He.

Table 3.2 lists a typical sample of experiment results from reactor feed (bypass) test and reactor effluent test as measured by GC/TCD. Reaction conditions were 300℃ and 50psig. Total flow rate was 645 sccm, flow rate of He is 590 sccm, gas hourly space velocity (GHSV) =2580 hr^{-1}. In order to ensure accuracy, every GC/TCD run was repeated.

Table 3.2 Sample Data of Methane Partial Oxidation Experiment

	#	Species	Retention time (s)	Peak area (mV ·s)	Composition (mole %)
Bypass Experiments	1	O_2	~174	176.8	1.20
		CH_4	~321	681.3	5.15
	2	O_2	~174	176.6	1.20
		CH_4	~321	677.7	5.12
Reactor Effluent	1	H_2	~121	0.6546	4.77
		O_2	~174	1.841	0.01
		CO	~183	12.84	0.08
		CH_4	~321	561.5	4.24
		CO_2	~797	146.4	0.78
	2	H_2	~121	0.8737	6.37
		O_2	~174	1.919	0.01
		CO	~183	12.68	0.08
		CH_4	~321	561.9	4.24
		CO_2	~797	149.7	0.80

Since each run was repeated, the mean was taken as the final result. The result is shown as Table 3.3.

Table 3.3 Sample Mean Composition - Reactor Feed and Effluent

	Species	Composition (mole fraction)
Reactants	O_2	1.20
	CH_4	5.14
Products	H_2	5.57
	O_2	0.01
	CO	0.08
	CH_4	4.24
	CO_2	0.79

From Table 3.3, the inlet CH_4/O_2 ratio = 5.14/1.20 = 4.28. The reacted O_2/reacted CH_4 = (1.20 - 0.01) / (5.14 - 4.24) = 1.32. The CH_4 conversion = (5.14 - 4.24) / 5.14 = 0.1751 or 17.51%.

3.2 Material (Mole) Balance

3.2.1 Carbon Balance

The overall reaction stoichiometry can be taken as:

$$CH_4 + (p+r+2s)/2\ O_2 \rightarrow pCO + qH_2 + rH_2O + sCO_2$$

The carbon atoms from CH_4 should convert to CO and CO_2, so the sum of CO moles and CO_2 moles should be close to the moles of converted CH_4. Such a carbon balance is a good test of the experimental method, as well as a test for any possible carbon

deposits on the catalyst. Figure 3.1 shows a typical sample carbon balance. Reaction conditions were 350 ℃ and 50 psig. Total flow rate=645 sccm, flow rate of He=590 sccm, GHSV = 2580 h^{-1}. The feed molar ratio CH_4/O_2=4.98.

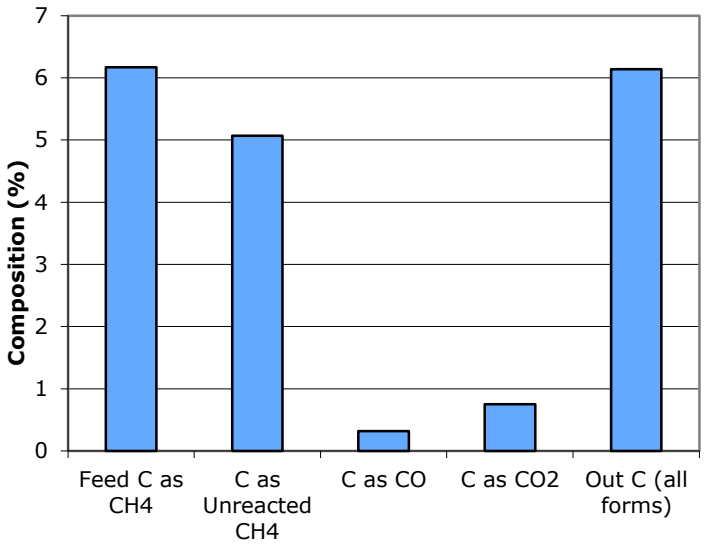

Figure 3.1 Typical experimental carbon balance

Outlet carbon (all forms) is the sum of C as unreacted CH_4, C as CO and C as CO_2. Figure 3.1 shows that the feed C is very close to that of outlet carbon. The carbon balance is very good. Actually, such good carbon balances were achieved thorough out the whole study. That means that carbon deposition on the catalyst surface is negligible.

3.2.2 Oxygen Balance

Although having no data of H_2O vapor content, it is estimated based on the O atom balance since O_2, CO and CO_2 are accurately measured, and O_2 is the only oxygen atom source in the feed. A sample is shown in Figure 3.2. Unlike the C atom, the O atom balance is exact by definition.

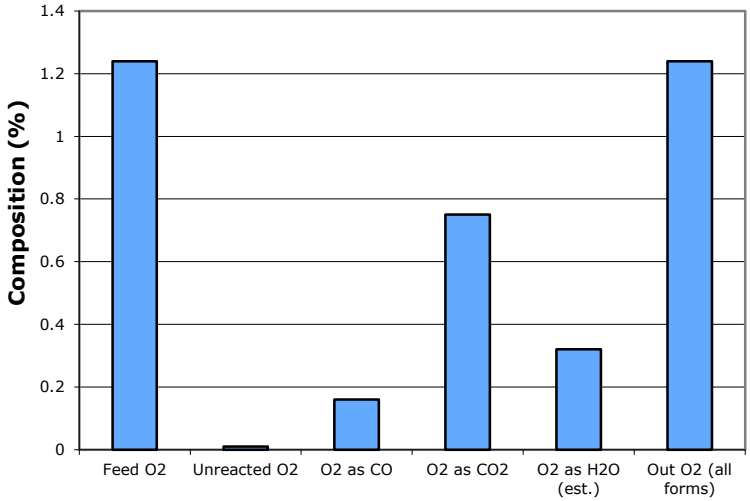

Figure 3.2 A sample of oxygen balance.

3.2.3 Hydrogen Balance

With the C and O atom balances complete, the H atom balance is determined. Since H_2O is estimated, and CH_4 measured, the concentration of H_2 is calculated. These estimated H_2 values can be compared to the experimental H_2. An acceptable comparison is a bonus since reliability of the H_2 data is not strong. Figure 3.3 presents the H atom balance with measured H_2 – an acceptable comparison.

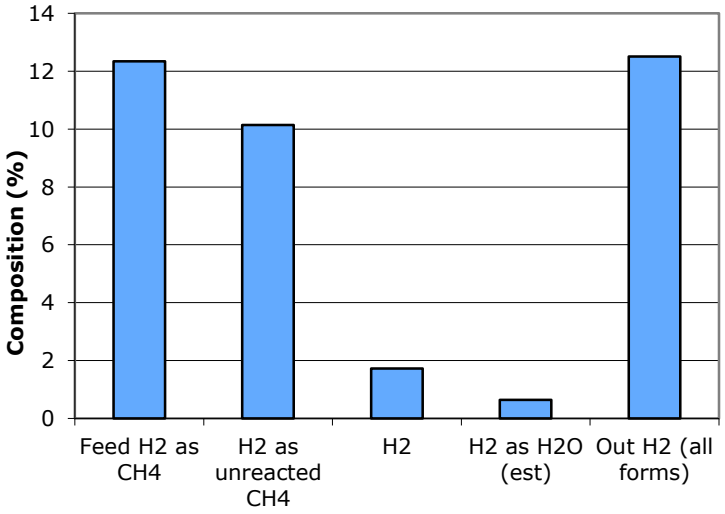

Figure 3.3 A sample of hydrogen balance.

From Figure 3.3, we could conclude that hydrogen balance is very good for this case. But for the whole study, hydrogen balance often does not perform well. The linear response of a thermal conductivity detector (TCD) assumes that the sample gases have a significantly lower thermal conductivity than the carrier gas. The carrier gas used in this study is He. But the thermal conductivity of H_2 is similar and slightly higher than He (e.g., He 0.142, H_2 0.168, CH_4 0.030, O_2 0.024 W/m-K at 25^{o}C.). That is why it is hard to get reliable H_2 mole fraction data. The result is a linear TCD response for H_2 in a He carrier up to a few mole percent [19]. This difficulty was observed in this study.

3.3 Stoichiometry

The overall reaction stoichiometry can be taken as:

$$CH_4 + (p+r+2s)/2\ O_2 \rightarrow pCO + qH_2 + rH_2O + sCO_2$$

To calculate all the stoichiometry coefficients:

$$(p + r + 2s)/2 = \frac{\text{Converted Moles of } O_2}{\text{Converted Moles of } CH_4} \tag{3.1}$$

Since there is a negligible change of total moles in current system as the feed is highly diluted by He (> 90%), then Equation 3.1 reduces to:

$$(p + r + 2s)/2 = \frac{\text{Feed } O_2 \text{ Fraction} - \text{Outlet } O_2 \text{ Fraction}}{\text{Feed } CH_4 \text{ Fraction} - \text{Outlet } CH_4 \text{ Fraction}} \tag{3.2}$$

In the same way, p and r could also be calculated as:

$$p = \frac{\text{Outlet CO Fraction}}{\text{Feed } CH_4 \text{ Fraction} - \text{Outlet } CH_4 \text{ Fraction}} \tag{3.3}$$

$$r = \frac{\text{Outlet } CO_2 \text{ Fraction}}{\text{Feed } CH_4 \text{ Fraction} - \text{Outlet } CH_4 \text{ Fraction}} \tag{3.4}$$

As mole fractions of CH_4, O_2, CO and CO_2 were precisely measured in experiments, the values of (p+r+2s)/2, p, and s are believed accurate. Then value of r could be determined. Since reliable H_2 mole fraction data cannot achieved from this study, q should be estimated from hydrogen balances.

CHAPTER 4

EXPERIMENTAL RESULTS AND DISCUSSION

4.1 Methane Conversion

To calculate methane conversions (X_A), we have

$$X_A = \frac{\text{Moles of Converted } CH_4}{\text{Moles of Feed } CH_4} \tag{4.1}$$

Since there is a negligible change of total moles in current system as the feed is highly diluted by He, then Equation 4.1 reduces to:

$$X_A = \frac{\text{Feed } CH_4 \text{ Mole Fraction} - \text{Outlet } CH_4 \text{ Mole Fraction}}{\text{Feed } CH_4 \text{ Mole Fraction}} \tag{4.2}$$

Equation 4.2 is used to calculate conversions CH_4 for all cases in this study.

4.1.1 Influence of Feed Molar Ratio on Methane Conversion

Experiments were run at 250 ℃, 275 ℃, 300 ℃, 325 ℃, 350 ℃ and 375 ℃. Reactor pressure is kept at 50 psig. The total flow rate is set at 645 sccm, with the flow rate of He of 590 sccm (more than 91% diluent). Based on the volume of the catalyst bed, the gas hourly space velocity (GHSV) is 2580 h^{-1}. All calculated methane conversions are shown as X_A vs. feed molar ratio CH_4/O_2 plots at each temperature.

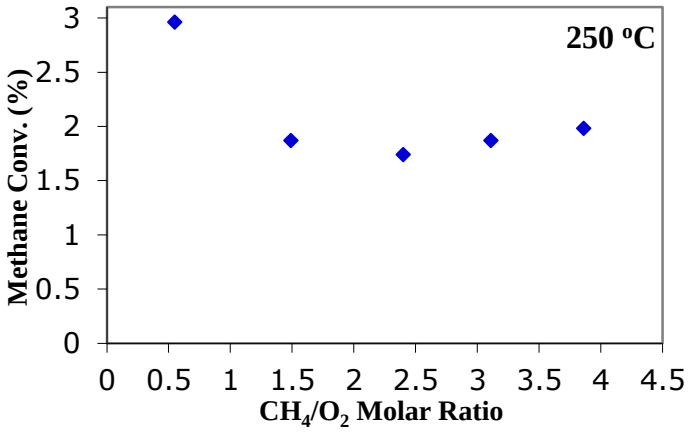

Figure 4.1 Conversion vs. molar ratio CH_4/O_2 at 250 ^oC.

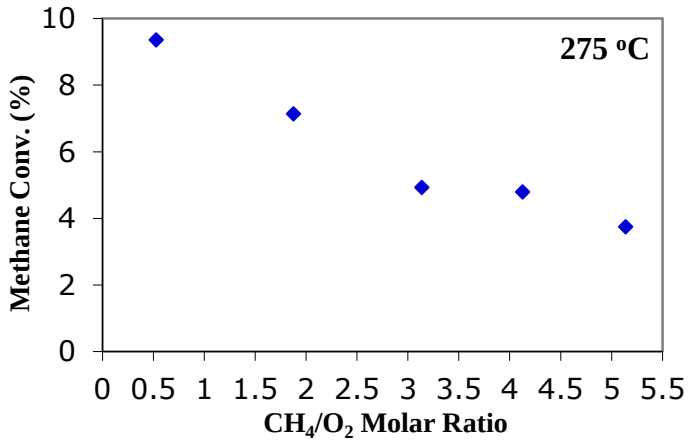

Figure 4.2 Conversion vs. molar ratio CH_4/O_2 at 275 ^oC.

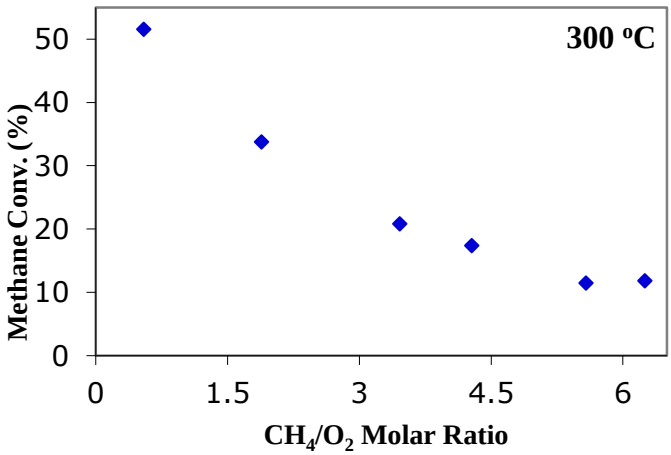

Figure 4.3 Conversion vs. molar ratio CH_4/O_2 at 300 ^oC.

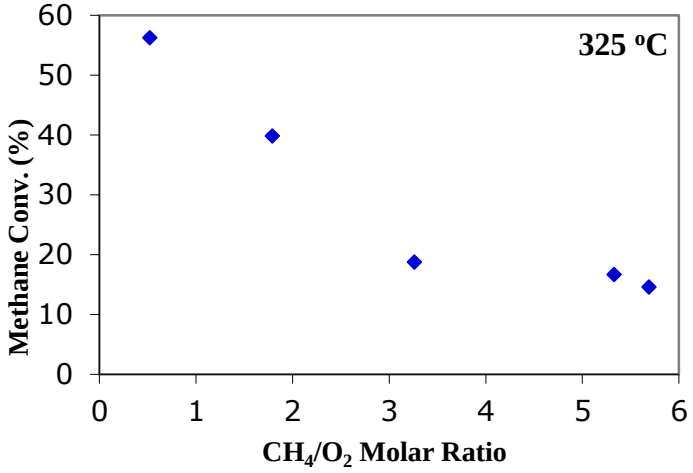

Figure 4.4 Conversion vs. molar ratio CH_4/O_2 at 325 ^oC.

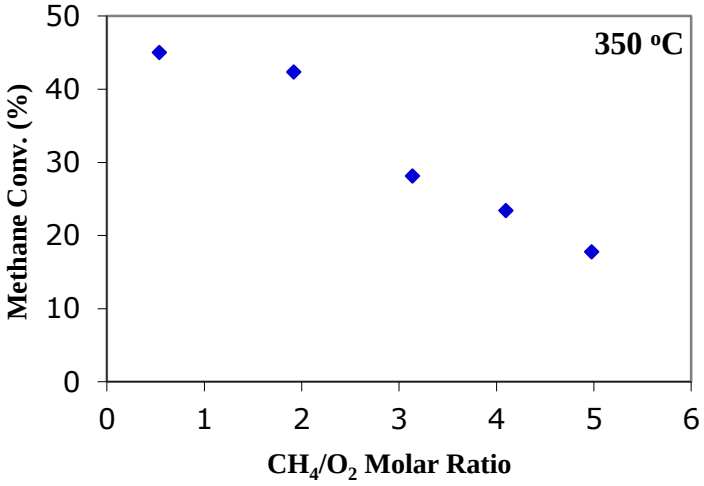

Figure 4.5 Conversion vs. molar ratio CH_4/O_2 at 350 ^oC.

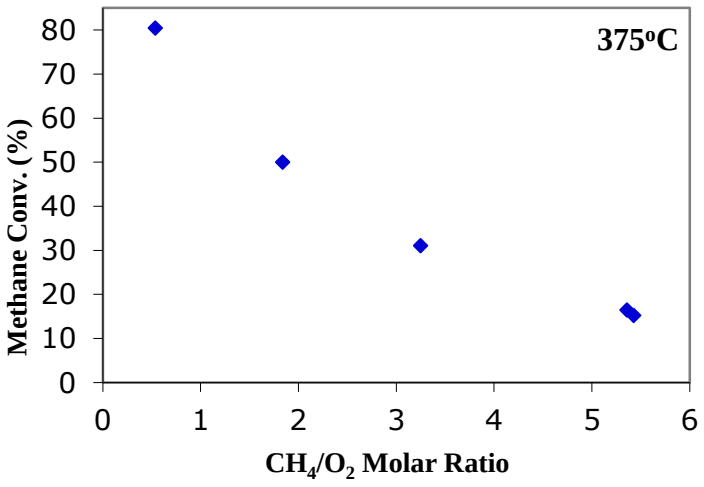

Figure 4.6 Conversion vs. molar ratio CH_4/O_2 at 375 ^oC.

Figures 4.1-4.6 show the different methane conversions at various molar ratios CH_4/O_2 under each temperature. The molar ratio CH_4/O_2 has a significant influence on methane conversion. Conversion decreases with increasing molar ratio CH_4/O_2. The higher the reaction temperature is, bigger is the drop.

4.1.2 Influence of Temperature on Methane Conversion

To investigate the influence of reaction temperature, some experiments were run at the same feed molar ratio of CH_4/O_2. Reaction pressure was kept at 50 psig. Total flow rate was 645 sccm, flow rate of He was 590 sccm, GHSV was 2580 /hr. Results are shown as Figures 4.7-4.9.

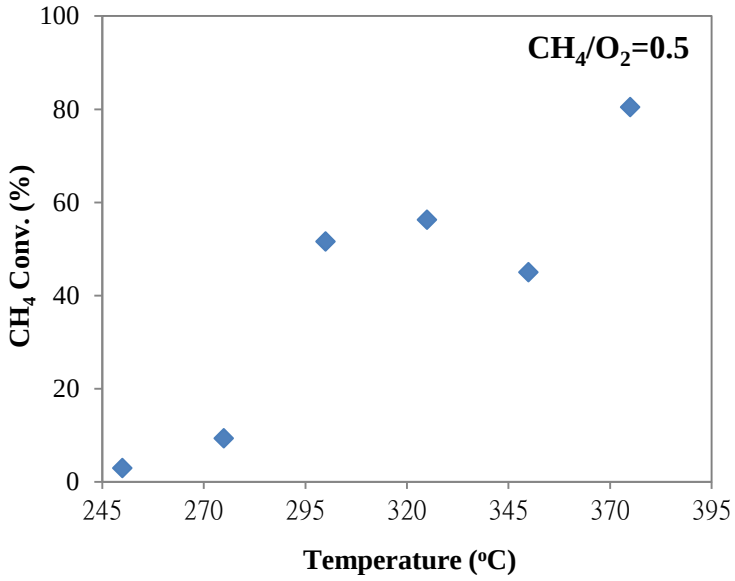

Figure 4.7 Conversion vs. temperature while molar ratio CH_4/O_2=0.5.

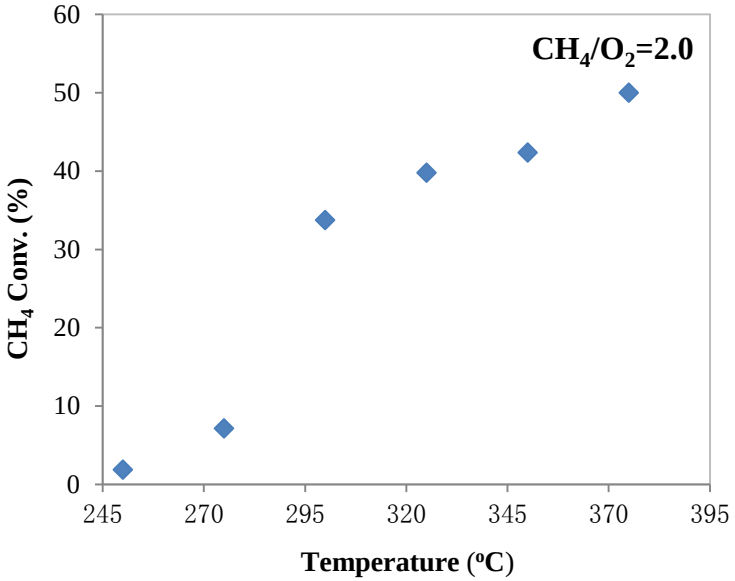

Figure 4.8 Conversion vs. temperature while molar ratio CH_4/O_2=2.0.

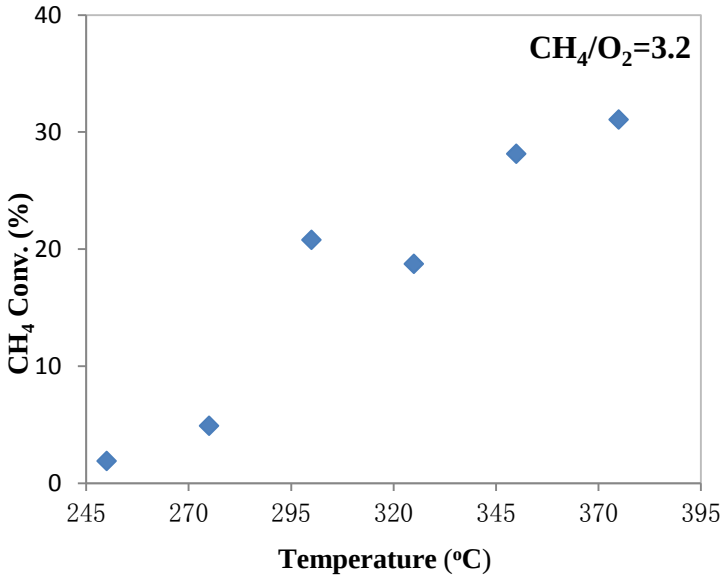

Figure 4.9 Conversion vs. temperature while molar ratio CH_4/O_2=3.2.

From Figures 4.7-4.9, the overall trend of methane conversion is higher with increasing temperature. Within the range of 270°C~320°C, CH_4 conversion increases fastest. The magnitude of the conversion increase is most evident at the lower feed CH_4/O_2 ratios.

4.1.3 Upper Limit of Methane Conversion

There is a theoretical upper limit to CH_4 conversion based on CH_4/O_2 feed molar ratio and the stoichiometry for total oxidation:

$$CH_4 + 2\ O_2 \rightarrow CO_2 + 2\ H_2O$$

For conversions:

$$X_A \equiv \frac{F_{Ao} - F_A}{F_{Ao}} \tag{4.3}$$

$$X_B \equiv \frac{F_{Bo} - F_B}{F_{Bo}} \tag{4.4}$$

where $A \equiv CH_4$, and $B \equiv O_2$, F_j = molar flow rate of species j, F_{jo} = molar feed rate of j, and X_j = conversion of j, and $MR \equiv F_{A0}/F_{B0}$.

Using the stoichiometry,

$$F_{B0} - F_B = 2(F_{A0} - F_A) \tag{4.5}$$

This is written as:

$$F_{B0}X_B = 2F_{A0}X_A \tag{4.6}$$

Therefore:

$$X_A = \frac{X_B}{2(F_{A0}/F_{B0})} = \frac{X_B}{2MR} \tag{4.7}$$

where $MR\ (Molar\ ratio) \equiv F_{A0}/F_{B0}$.

Figure 4.10 shows a comparison between the total oxidation methane conversion and a sample of experiment conversion (375 ^{o}C). The experimental data certainly follow this general pattern that, as MR increases, the CH_4 conversion should decrease as 1/MR.

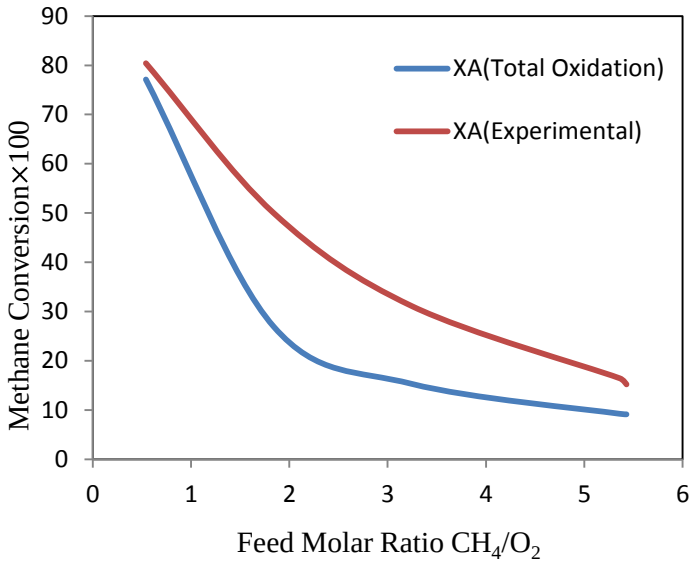

Figure 4.10 Total oxidation conversion vs. 375 ^{o}C experimental conversion.

From Figure 4.10, the experimental data certainly follow this general pattern that, as MR increases, the CH_4 conversion should decrease as 1/MR. The blue curve shows the maximum CH_4 conversion that could be observed as a function of MR, assuming complete oxidation to CO_2 and H_2O with stoichiometric coefficient of O_2 equaling to 2. If altering the stoichiometry to a syngas formulation, a smaller stoichiometric coefficient of O_2 would be achieved (red curve). It's clear that any syngas stoichiometry will give a curve above the total oxidation curve.

4.2 Selectivity of Product

The selectivity indicates how much of the converted methane goes to specific product,

$$\text{Selectivity of product X} = \frac{\text{Moles of Product X}}{\text{Moles of Converted } CH_4} \quad (4.8)$$

Since there is a negligible change in total moles as the feed is highly diluted by He, then product selectivities can be obtained directly from measured mole fractions.

$$\text{Selectivity of product X} = \frac{\text{Outlet Product X Mole Fraction}}{\text{Feed } CH_4 \text{ Mole fraction} - \text{Outlet } CH_4 \text{ Mole fraction}} \quad (4.9)$$

Based on Equation 4.9, the selectivities of CO, H_2 and CO_2 are estimated. Results are shown in Figures 4.11-4.13 following graphics. The lines connecting the markers in these plots are used only for the sake of clarity since the plot areas very busy.

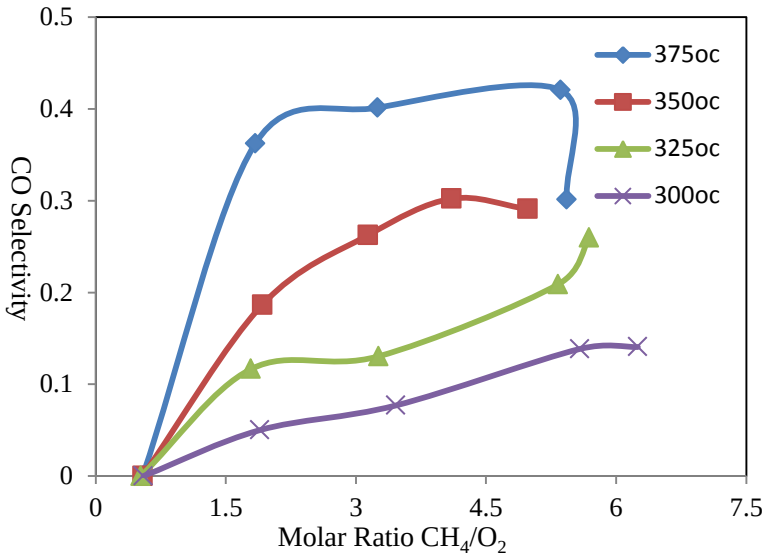

Figure 4.11 CO selectivity vs. molar ratio CH_4/O_2. There was no detectable CO generated at 250 ^oC or 275 ^oC.

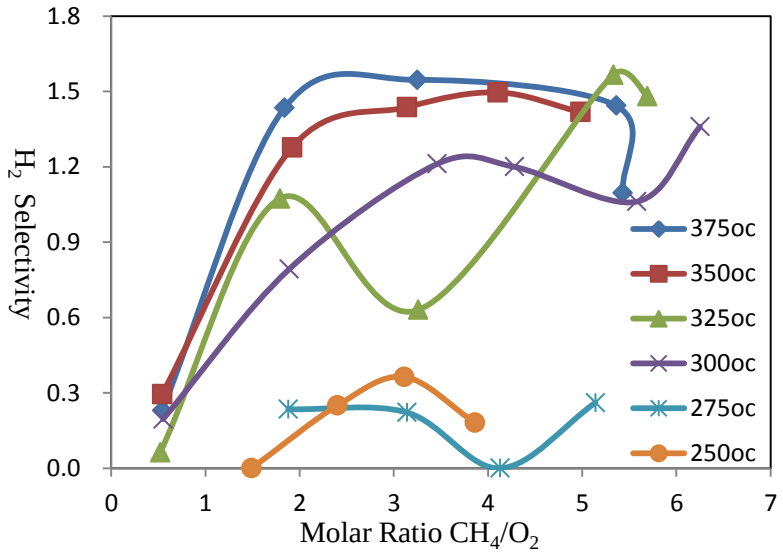

Figure 4.12 H_2 selectivity vs. molar ratio CH_4/O_2.

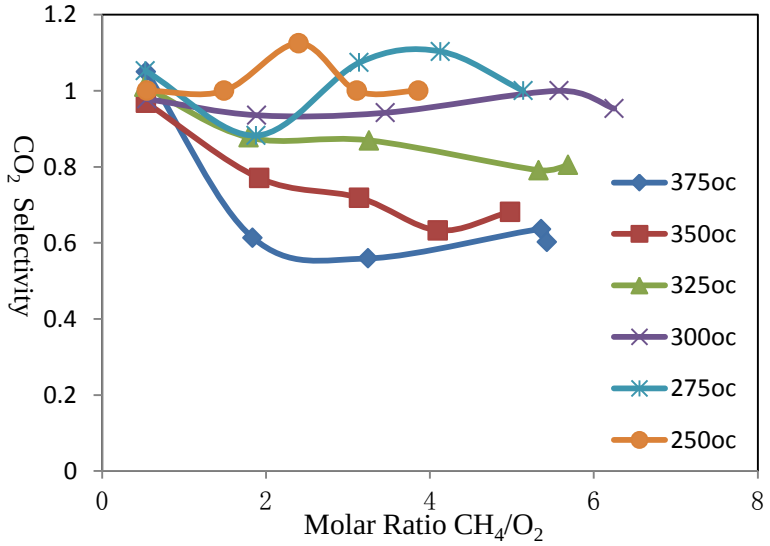

Figure 4.13 CO_2 selectivity vs. molar ratio CH_4/O_2.

From Figures 4.11-4.13, the selectivities of CO and H_2 increase with increasing molar ratio CH_4/O_2. Also, higher selectivities of CO and H_2 are achieved at higher temperature. From Figure 4.12, the selectivity of CO_2 is approximately 1.0 at 250 ^oC, 275 ^oC and 300 ^oC over the range of molar ratios. The selectivity of CO_2 deceases with

increasing molar ratio when reaction temperature is above 325 ^{o}C. Moreover, higher reaction temperature would lead to a lower CO_2 selectivity. Such findings are valuable since it is desirable to produce a synthesis gas as rich as possible in H_2 and CO.

4.3 Discussion of Stoichiometry

Use Equation 3.4 and the method described in Section 3.3, the stoichiometry coefficients are estimated for all cases. These results for most runs are shown as Table 4.1.

Table 4.1 Stoichiometry Coefficient

T	Feed CH_4/O_2	(p+r+2s)/2	p	q	r	s
375 °C	0.54	1.9353	0.0000	0.2302	1.7698	1.0504
	1.84	1.0773	0.3623	1.4348	0.5652	0.6135
	3.25	0.9868	0.4013	1.5461	0.4539	0.5592
	5.36	1.1250	0.4205	1.4432	0.5568	0.6364
	5.43	1.2048	0.3012	1.0964	0.9036	0.6024
350 °C	0.54	1.8211	0.0000	0.2947	1.7053	0.9684
	1.92	1.2249	0.1866	1.2775	0.7225	0.7703
	3.14	1.1313	0.2625	1.4375	0.5625	0.7188
	4.1	1.0360	0.3022	1.4964	0.5036	0.6331
	4.98	1.1182	0.2909	1.4182	0.5818	0.6818
325 °C	0.52	1.9789	0.0000	0.0632	1.9368	1.0105
	1.79	1.3988	0.1166	1.0736	0.9264	0.8773
	3.26	1.6196	0.1304	0.6304	1.3696	0.8696
	5.33	1.1222	0.2111	1.5667	0.4333	0.8000
	5.69	1.1948	0.2597	1.4805	0.5195	0.8052
300 °C	0.55	1.8804	0.0000	0.1957	1.8043	0.9783
	1.89	1.5643	0.0500	0.7929	1.2071	0.9357
	3.46	1.3750	0.0769	1.2115	0.7885	0.9423
	4.28	1.3222	0.0889	1.2000	0.8000	0.8778
	5.58	1.5385	0.1385	1.0615	0.9385	1.0000
	6.25	1.3438	0.1406	1.3594	0.6406	0.9531
275 °C	0.53	2.2632	0.0000	-0.4211	2.4211	1.0526
	1.88	1.7647	0.0000	0.2353	1.7647	0.8824
	3.14	1.9630	0.0000	0.2222	1.7778	1.0741
	4.13	2.1034	0.0000	0.0000	2.0000	1.1034
	5.14	1.8696	0.0000	0.2609	1.7391	1.0000
250 °C	0.55	2.6000	0.0000	-1.2000	3.2000	1.0000
	1.49	2.0000	0.0000	0.0000	2.0000	1.0000
	2.4	2.0000	0.0000	0.2500	1.7500	1.1250
	3.11	1.8182	0.0000	0.3636	1.6364	1.0000
	3.86	1.9091	0.0000	0.1818	1.8182	1.0000

Note: As experimental mole fractionS of H_2 are not fully reliable, the H_2 mole fractions shown are calculated based on an H atom balance. Thus, all elements are balanced. But two cases at 250 °C and 275 °C indicate negative H_2 mole fractions. This likely indicates an error in one of the other species.

A closer examination of the values in Table 4.1 reveals that, for each product, the average values of the stoichiometry coefficients are effectively functions only of temperature (only for Feed $CH_4/O_2>1$). For example, at 375 ^oC, the average value of the CO stoichiometry coefficient is (0.3623+0.4013+0.4205+0.3012)/4=0.3713. These results are listed in Table 4.2.

Table 4.2 Stoichiometry Coefficient vs. Temperature

T(^{o}C)	**T(k)**	**Average Value of (p+r+2s)/2**	**Average Value of p**	**Average Value of q**	**Average Value of s**
375	648	1.0985	0.3713	1.3801	0.6029
350	623	1.1276	0.2605	1.4074	0.7010
325	598	1.3338	0.1795	1.1878	0.8380
300	573	1.4287	0.0990	1.1251	0.9418
275	548	1.9252	0	0.1796	1.0150
250	523	1.9318	0	0.1989	1.0313

Based on Table 4.2, Figures 4.14-4.17 illustrate how the average values of stoichiometry coefficients vary linearly with temperature.

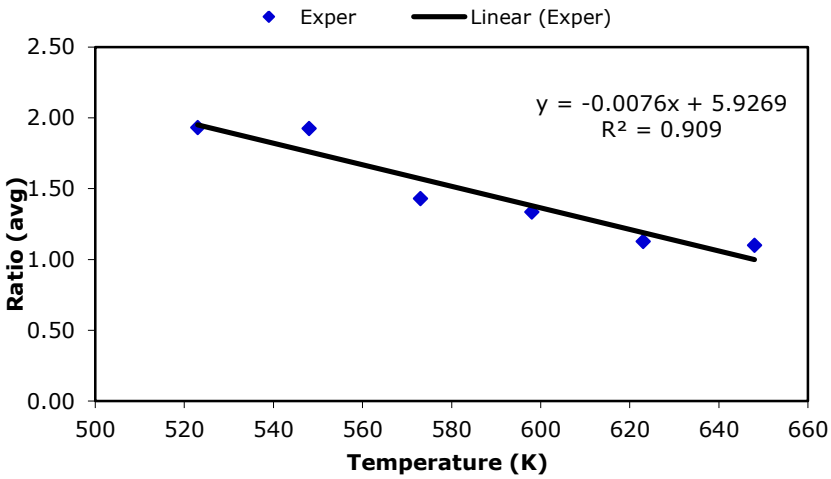

Figure 4.14 Avg. stoich. O_2/CH_4 ratio (feed $CH_4/O_2 > 1$).

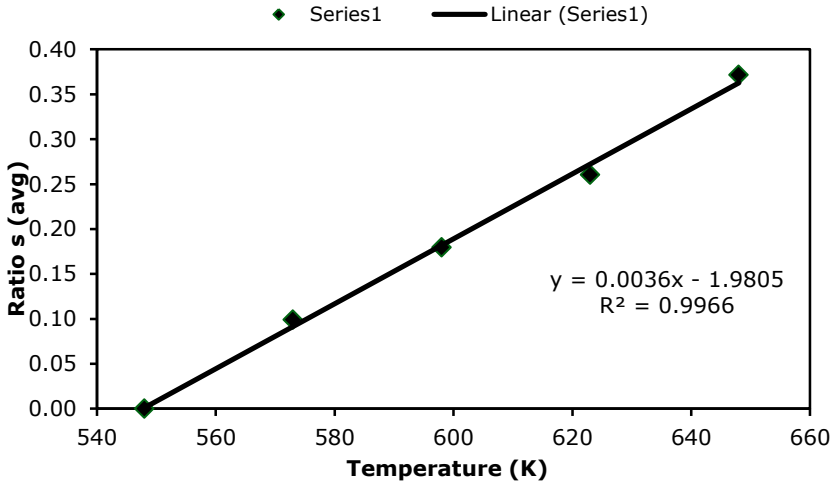

Figure 4.15 Avg. stoich. CO/CH_4 ratio (feed $CH_4/O_2 > 1$).

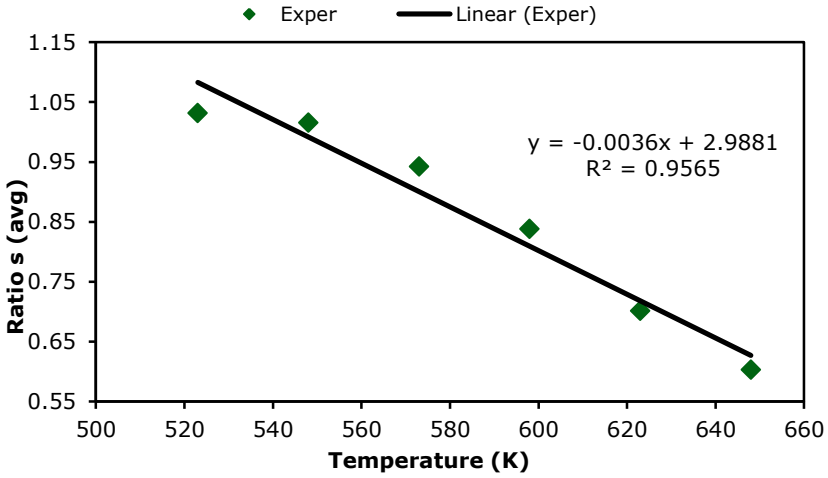

Figure 4.16 Avg. stoich. CO_2/CH_4 ratio (feed $CH_4/O_2 > 1$).

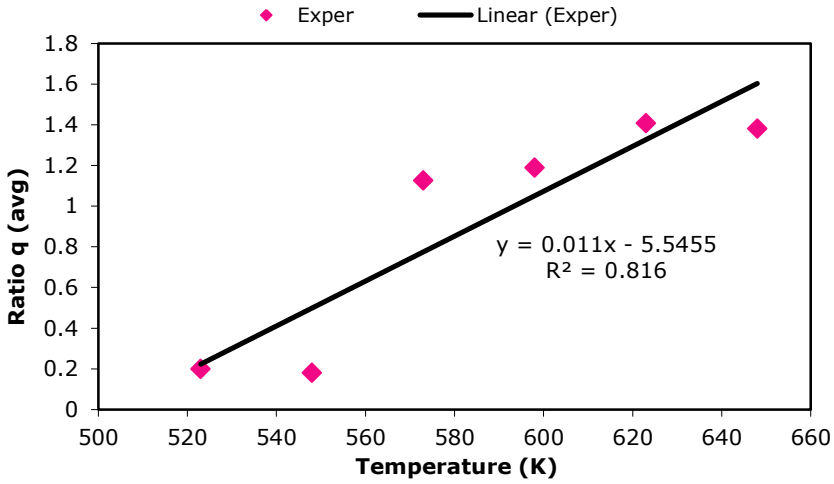

Figure 4.17 Avg. stoich. H_2/CH_4 ratio (feed $CH_4/O_2 > 1$).

From Figures 4.14–4.17, as strong linear relationships are shown between stoichiometry coefficients and reaction temperature, this indicates that the reaction mechanism responsible for all the products is complex, and is changing with temperature.

4.4 Preferred Reaction Condition for Synthesis Gas Production

The focus of this study is the conversion of methane into syngas. Therefore, a high methane conversion, high selectivities of CO and H_2, and low selectivity of CO_2 are all desirable. Based on the accumulated data for methane conversion and product selectivity shown above, higher reaction temperature is conducive to both higher methane conversion and selectivities to CO and H_2. But the influences of molar ratio CH_4/O_2 on methane conversion and product selectivities are different, as summarized Figure 4.18.

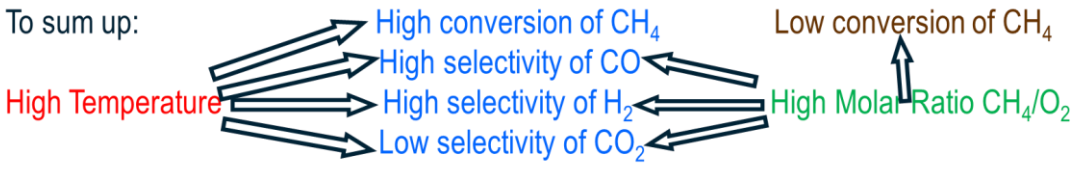

Figure 4.18 Influences of temperature and molar ratio CH_4/O_2.

Figure 4.18 suggests that the preferred operating conditions for syngas production should be based on an optimization. To find the best reaction condition, one approach would be to satisfy the requirement of high CO and H_2 selectivities as long as the CH_4 conversion is acceptable. Because unreacted methane could be separated from the reactor effluent and then recycled to the reactor feed. Additional space time in the reactor might also be used. Therefore, a molar ratio CH_4/O_2=2.0 at 375 ^oC is recommended.

CHAPTER 5

METHANE CONVERSION MODEL

5.1 Model Selection and Derivation

5.1.1 Model Selection

Data in Chapter 4 show that the methane conversions are sufficiently high (> 10%) that a simple differential reactor model is not appropriate. Rather, an integral packed bed reactor (PBR) model is used. It begins with:

$$r_A' = \frac{dF_A}{dW} \tag{5.1}$$

where A is methane, r_A' is the molar reaction rate (based on catalyst mass), W is mass of catalyst, and F_A is methane molar flow rate.

5.1.2 Model Derivation

The global reaction can be written as:

$$CH_4 + bO_2 \rightarrow cCO + dH_2 + eCO_2 + fH_2O$$

where A is assigned to CH_4, and B is assigned to O_2. This is equivalent to the stoichiometry shown in Chapters 3 and 4; e.g., b = (p+r+2s)/2. A global reaction rate form, sometimes called a power law, is assumed:

$$r_A' = kC_A^{\alpha}C_B^{\beta} \tag{5.2}$$

where k is the rate constant, and C_j are molar gas-phase concentrations and orders α and β are to be determined. The immediate objective is to derive F_A (molar rate of A), C_A, and C_B in terms of mole fraction y_A since y_A, the mole fraction of CH_4, is directly measured and is of key interest in determining the conversion of methane.

The volumetric flow rate of gas v depends on local temperature T, pressure P, and total molar rate F_T. Subscript o refers to the feed condition. Based on the ideal gas law,

$$v = v_0 \left(\frac{P_0}{P}\right)\left(\frac{T}{T_0}\right)\left(\frac{F_T}{F_{T0}}\right) \tag{5.3}$$

As the feed reactants are highly diluted by He (> 90%), $F_T \approx F_{To}$. In order to avoid a significant pressure drop across the catalyst bed, the catalyst was loaded into the reactor as broken pellets. This resulted $P \approx P_o$. Then, Equation 5.3 reduces to:

$$v = v_0 \left(\frac{T}{T_0}\right) \tag{5.4}$$

For the reactants molar flow rates, F_B depends on stoiciometry and the consumption of A:

$$F_B = F_{B0} - b(F_{A0} - F_A) \tag{5.5}$$

The flow rates F_A and F_B relate to the total F_T using the mole fractions y_j.

$$F_A = y_A F_T \text{ and } F_B = y_B F_T \tag{5.6}$$

For the reactants concentrations, using the ideal gas law:

$$C_A = \frac{P}{RT} y_A \tag{5.7}$$

where R is the ideal gas constant.

Using Equation 5.5, the mole fraction of B is:

$$y_B = \frac{F_B}{F_T} = \frac{F_{B0} - b(F_{A0} - F_A)}{F_T} \tag{5.8}$$

Due to high dilution, $F_T \approx F_{To}$. Equation 5.8 becomes:

$$y_B = \frac{F_{B0}}{F_{T0}} - b\left(\frac{F_{A0}}{F_{T0}}\right) + b\left(\frac{F_A}{F_{T0}}\right) = y_{B0} - by_{A0} + by_A \tag{5.9}$$

Defining $y_0 = \left(\frac{y_{B0}}{b} - y_{A0}\right)$, Equation 5.9 becomes:

$$y_B = b(y_0 + y_A) \tag{5.10}$$

The molar concentration of B is now:

$$C_B = \frac{F_B}{v} = \frac{y_B F_T}{v} = y_B \frac{P}{RT} \tag{5.11}$$

Substituting Equation 5.10 into 5.11 yields:

$$C_B = (y_0 + y_A)\frac{bP}{RT} \tag{5.12}$$

Substituting C_A and C_B (Equations 5.7 and 5.11, respectively) into Equation 5.2, we have:

$$-r_A' = k\left(\frac{P}{RT}\right)^{\alpha+\beta} y_A^{\alpha}(y_0 + y_A)^{\beta} b^{\beta} \tag{5.13}$$

Using Equation 5.6 together with $F_T \approx F_{To}$,

$$F_A \approx y_A F_T \tag{5.14}$$

Finally, substituting Equations 5.13 and 5.14 into the PBR species balance (Equation 5.1) yields a working model that could be used directly for data regression.

$$\frac{dy_A}{dW} = \frac{-k}{F_{T0}}\left(\frac{P}{RT}\right)^{\alpha+\beta} y_A^{\alpha}(y_0 + y_A)^{\beta} b^{\beta} \tag{5.15}$$

To obtain a better perspective, Equation 5.15 can be put in terms of CH_4 conversion X_A. Using the definition, $X_A \equiv (F_{A0} - F_A)/F_{A0}$, $F_A = y_A F_{To}$, and $F_T \approx F_{To}$, the y_A is:

$$y_A = \frac{F_{A0}(1 - X_A)}{F_{T0}} \tag{5.16}$$

Substituting Equation 5.16 into 5.15, together with manipulations, the working model becomes:

$$\frac{dX_A}{dW} = \frac{k}{F_{A0}}\left(\frac{P y_{A0}}{RT}\right)^{\alpha+\beta} (1 - X_A)^{\alpha}\left(\frac{y_{B0}}{b y_{A0}} - X_A\right)^{\beta} b^{\beta} \tag{5.17}$$

The final form of the methane conversion model is Equation 5.17. The quantities W, F_{T0}, P, T, y_A, and y_0 are all known. The parameters k, α and β are all unknown. The value of b could be determined by:

$$b = \frac{\text{Moles of Converted } O_2}{\text{Moles of Converted } CH_4} \tag{5.18}$$

Since there is a negligible change of total moles in current system as the feed is highly diluted by He, then Equation 5.18 reduces to:

$$b = \frac{\text{Feed } O_2 \text{Mole Fraction} - \text{Outlet } O_2 \text{Mole Fraction}}{\text{Feed } CH_4 \text{ Mole Fraction} - \text{Outlet } CH_4 \text{ Mole Fraction}} \tag{5.19}$$

Equation 5.19 is used to calculate the value of b for all cases in this study. These values are presented earlier in Chapter 4 as (p+r+2s)/2.

The approach will be to numerically integrate Equation 5.17 with assumed values of k, α and β for a given run. The calculated X_A is compared to the experimental X_A. If the two X_A cannot match well, the assumed values of k, α and β are altered, until a good fit is found. This procedure is repeated over all the experimental runs.

5.2 Model Testing

As a reasonable start, the orders α and β of the reaction rate were both set to be one. Equation 5.2 becomes:

$$r_A' = kC_AC_B \tag{5.20}$$

The second assumption is the value of k, which is assumed to be temperature dependent.

5.2.1 Steady Total Flow Rate

A typical sample case is temperature at 325 ^{o}C, feed molar ratio CH_4/O_2 of 3.26, reaction pressure at 50 psig, total flow rate is 645 sccm, flow rate of He is 590 sccm, and GHSV is 2580 h^{-1} and W=9.91 gram. Experimental methane conversion is 18.73%. The assumed value of k is1.0×10^{6} cm^{6}/ (min gram mol).

The solution tool used to integrate Equation 5.17 for the runs is the software package Polymath®. The calculated methane conversion is 5.05%, which is quite too low compared with the experimental methane conversion. Different k values are tried until the difference between the predicted and experimental conversions is small enough.

Finally, when k=1.1×10^{7} cm^{6}/ (min gram mol), the predicted X_A=18.01%, which is very close to the experimental methane conversion X_A=18.73%. Figure 5.1 shows the original Polymath® code for solving this case, with assumptions, α=1, β=1 and k=1.1×10^{7}. Four more runs with various molar ratios of CH_4/O_2 were also made at 325 ^{o}C. “Best fit” k values are similarly estimated.

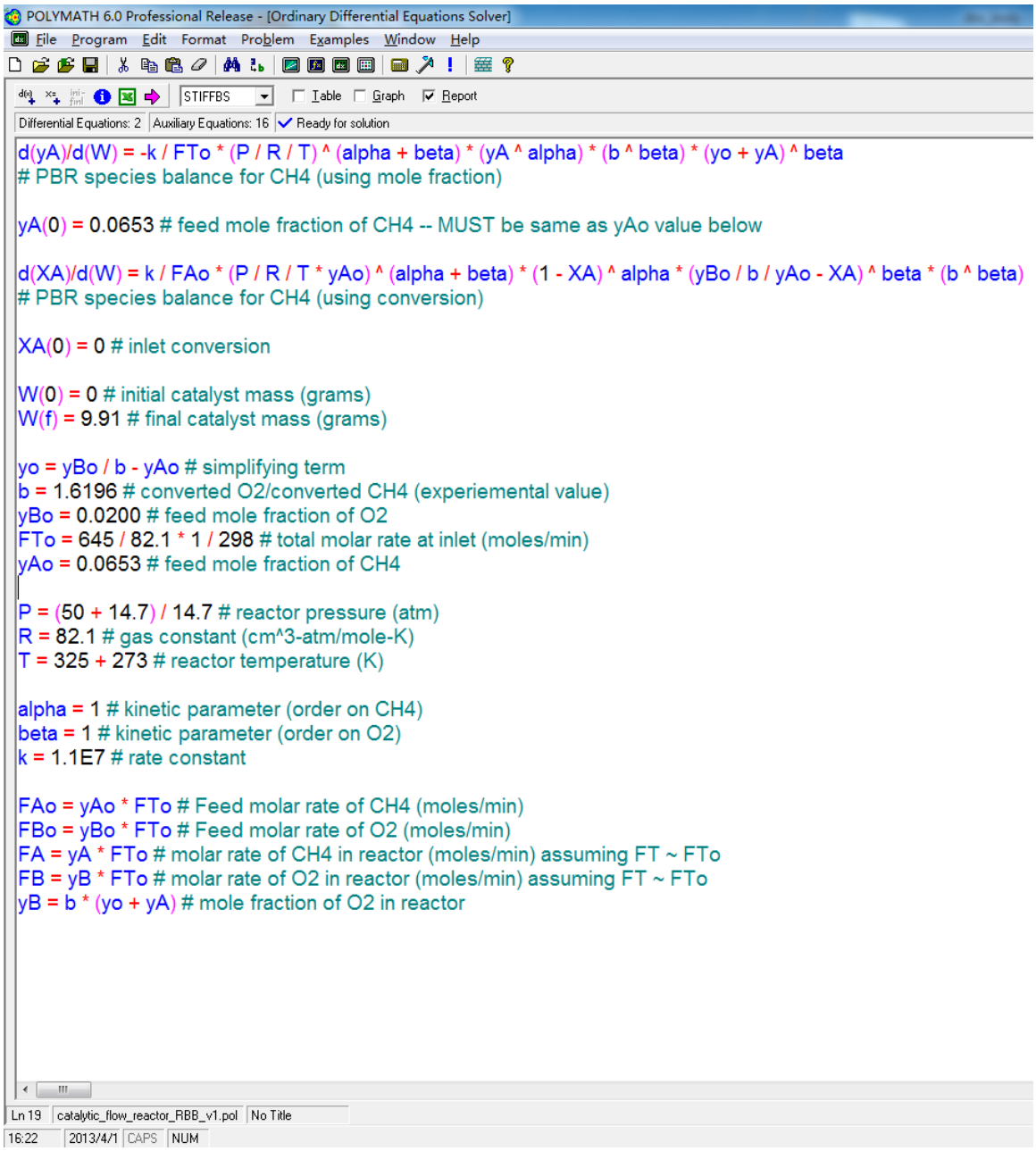

Figure 5.1 Polymath code for the sample case for integration of Eq. 5.17.

Polymath® generates a report (Figures 5.2-5.3) showing the detailed solution.

POLYMATH Report
Ordinary Differential Equations

Calculated values of DEQ variables

	Variable	Initial value	Minimal value	Maximal value	Final value
1	W	0	0	9.91	9.91
2	yA	0.0653	0.0535368	0.0653	0.0535368
3	XA	0	0	0.1801402	0.1801402
4	yAo	0.0653	0.0653	0.0653	0.0653
5	b	1.6196	1.6196	1.6196	1.6196
6	yBo	0.02	0.02	0.02	0.02
7	FTo	0.0263633	0.0263633	0.0263633	0.0263633
8	yo	-0.0529513	-0.0529513	-0.0529513	-0.0529513
9	P	4.401361	4.401361	4.401361	4.401361
10	R	82.1	82.1	82.1	82.1
11	T	598.	598.	598.	598.
12	alpha	1.	1.	1.	1.
13	beta	1.	1.	1.	1.
14	k	1.1E+07	1.1E+07	1.1E+07	1.1E+07
15	FAo	0.0017215	0.0017215	0.0017215	0.0017215
16	FBo	0.0005273	0.0005273	0.0005273	0.0005273
17	FA	0.0017215	0.0014114	0.0017215	0.0014114
18	yB	0.02	0.0009484	0.02	0.0009484
19	FB	0.0005273	2.5E-05	0.0005273	2.5E-05

Differential equations

1 d(yA)/d(W) = -k / FTo * (P / R / T) ^ (alpha + beta) * (yA ^ alpha) * (b ^ beta) * (yo + yA) ^ beta
2 d(XA)/d(W) = k / FAo * (P / R / T * yAo) ^ (alpha + beta) * (1 - XA) ^ alpha * (yBo / b / yAo - XA) ^ beta * (b ^ beta)

Figure 5.2 Polymath report (a).

Explicit equations

1 yAo = 0.0653
feed mole fraction of CH4

2 b = 1.6196
converted O2/converted CH4 (experiemental value)

3 yBo = 0.0200
feed mole fraction of O2

4 FTo = 645 / 82.1 * 1 / 298
total molar rate at inlet (moles/min)

5 yo = yBo / b - yAo
simplifying term

6 P = (50 + 14.7) / 14.7
reactor pressure (atm)

7 R = 82.1
gas constant (cm^3-atm/mole-K)

8 T = 325 + 273
reactor temperature (K)

9 alpha = 1
kinetic parameter (order on CH4)

10 beta = 1
kinetic parameter (order on O2)

11 k = 1.1E7
rate constant

12 FAo = yAo * FTo
Feed molar rate of CH4 (moles/min)

13 FBo = yBo * FTo
Feed molar rate of O2 (moles/min)

14 FA = yA * FTo
molar rate of CH4 in reactor (moles/min) assuming FT ~ FTo

15 yB = b * (yo + yA)
mole fraction of O2 in reactor

16 FB = yB * FTo
molar rate of O2 in reactor (moles/min) assuming FT ~ FTo

General

Total number of equations	18
Number of differential equations	2
Number of explicit equations	16
Elapsed time	1.157 sec
Solution method	STIFFBS
Independent variable accuracy. eps	.00001
First stepsize guess. h1	.001
Minimum allowed stepsize. hmin	.00001
Good steps	163
Bad steps	0

Figure 5.3 Polymath report (b).

The Polymath® report shows a good fit with the experimental methane conversion for this case with α=1, β=1 and k=1.1×10^7. Moreover, after further testing, we are satisfied with the other four results. Figure 5.4 shows the excellent comparison between experimental methane conversions and model-simulated conversions at 325 ^{o}C for five different feed CH_4/O_2 ratios, with α=1, β=1and k=1.1×10^7 cm^6/ (min gram mol).

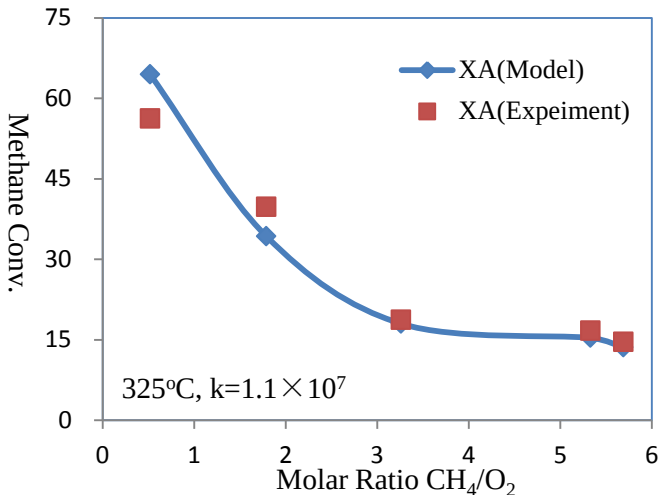

Figure 5.4 Model X_A vs. experimental X_A at 325 ^{o}C.

Figure 5.4 shows that the model with assumptions α=1, β=1and k=1.1×10^7 cm^6/ (min gram mol) works well. Similarly, for runs at other temperatures, α=1 and β=1 were used. Values for k were assumed at 250 ^{o}C , 275 ^{o}C , 300 ^{o}C , 350 ^{o}C and 375 ^{o}C until the "best fits" were found. Comparisons between experimental CH_4 conversions and model conversions for the other five temperatures are shown as Figures 5.5-5.9.

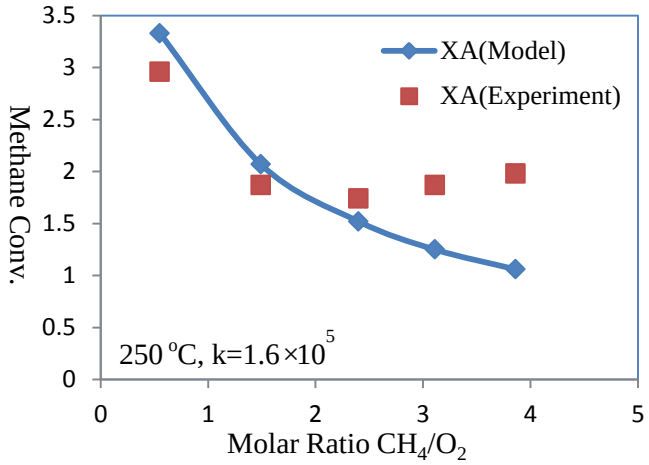

Figure 5.5 Model X_A vs. experimental X_A at 250 °C.

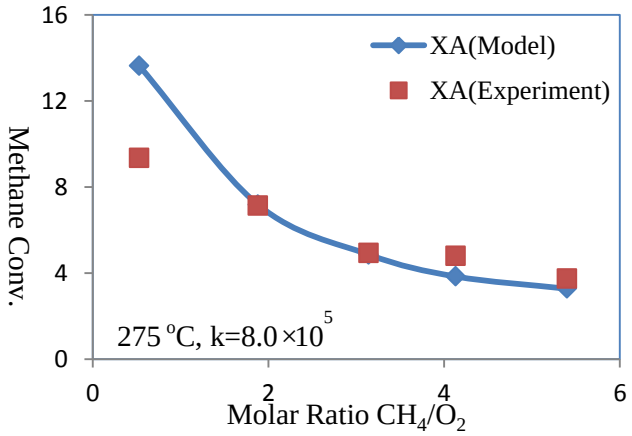

Figure 5.6 Model X_A vs. experimental X_A at 275 °C.

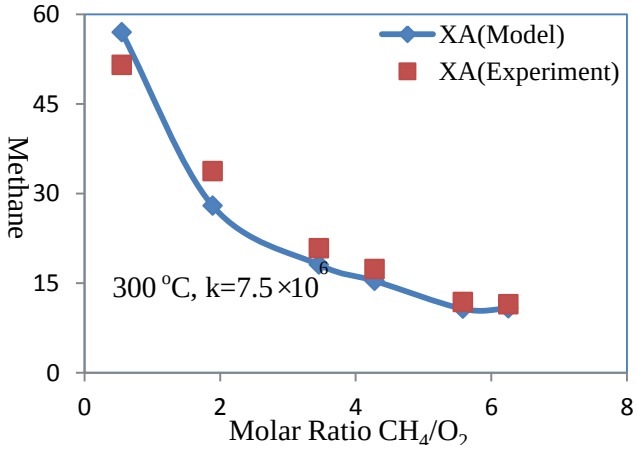

Figure 5.7 Model X_A vs. experimental X_A at 300 °C.

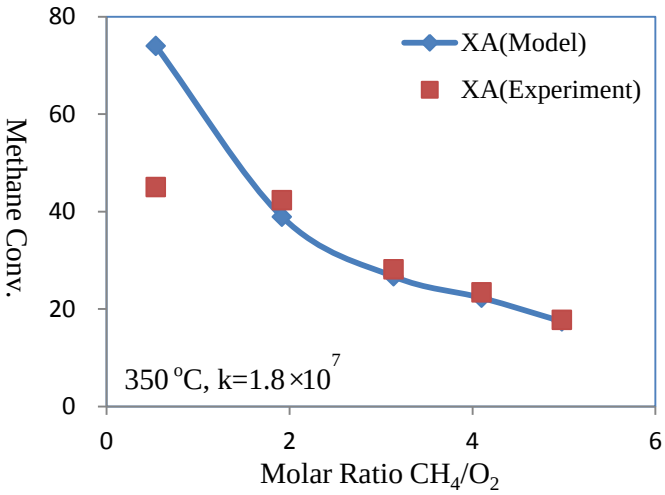

Figure 5.8 Model X_A vs. experimental X_A at 350 °C.

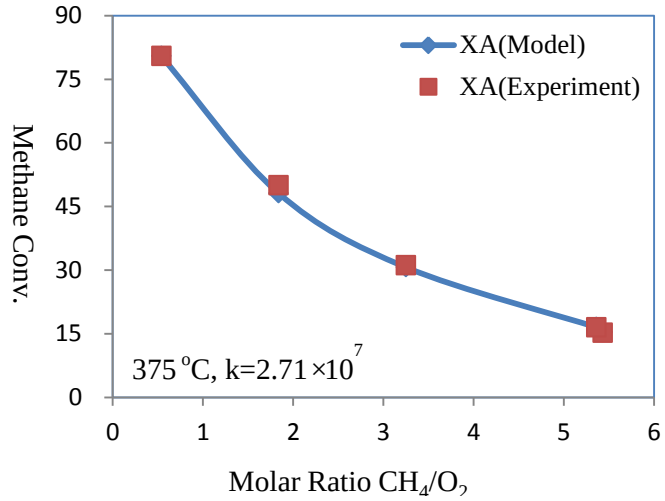

Figure 5.9 Model X_A vs. experimental X_A at 375 °C.

Figures 5.4-5.9 (constant total flow rate for all plots) show us a generally good fit between model-simulated CH_4 conversion and experimental CH_4 conversion assuming both α and β are 1. Trial-and-error process estimates k, for the given six temperatures, that predicts X_A values similar to observed X_A for each molar ratio of CH_4/O_2. In the next section, the dependence of the k values is examined as a function of temperature.

5.2.2 Uncertainty

The kinetic modeling needs an indication of the uncertainty (precision) in the experimental data. Since the modeling involves CH_4 conversion (X_A), which is a calculated quantity based on two different experimental values, a propagation of errors analysis is appropriate. The +/- uncertainty in X_A is given by σ_{XA}.

$$X_A = \frac{y_{Ao} - y_A}{y_{Ao}} = 1 - \frac{y_A}{y_{Ao}} \tag{5.21}$$

$$\left(\sigma_{X_A}\right)^2 = \left(\frac{\partial_{X_A}}{y_{Ao}}\right)^2 \left(\sigma_{y_{Ao}}\right)^2 + \left(\frac{\partial_{X_A}}{y_A}\right)^2 \left(\sigma_{y_A}\right)^2 \tag{5.22}$$

Applying the propagation equation:

$$\left(\sigma_{X_A}\right)^2 = \left(\frac{y_A}{y_{Ao}^2}\right)^2 \left(\sigma_{y_{Ao}}\right)^2 + \left(-\frac{1}{y_{Ao}}\right)^2 \left(\sigma_{y_A}\right)^2 \tag{5.23}$$

Based on Equation 5.23, σ_{XA} could be determined for all cases at 350 ^oC. All data are listed in Table 5.1.

Table 5.1 Experimental Methane Conversion Uncertainty Data

Feed CH_4/O_2	Out. CH_4 Mole Fraction (y_A)	In. CH_4 Mole Fraction (y_{Ao})	CH4 Fractional Conversion	Uncertainty of y_A (σ_{yA}) (2% of y_A)	Uncertainty of y_{Ao} (σ_{yA0}) (2% of y_{Ao})	Uncertainty of X_A (σ_{XA})
0.54	0.0118	0.0212	0.4434	0.0006	0.0011	0.0394
1.92	0.0284	0.0493	0.4239	0.0014	0.0025	0.0407
3.14	0.0409	0.0569	0.2812	0.0021	0.0028	0.0508
4.10	0.0456	0.0456	0.2336	0.0023	0.0030	0.0542
4.98	0.0507	0.0617	0.1783	0.0025	0.0031	0.0581

Based on Table 5.1, Figure 5.10 is made for the uncertainties analysis.

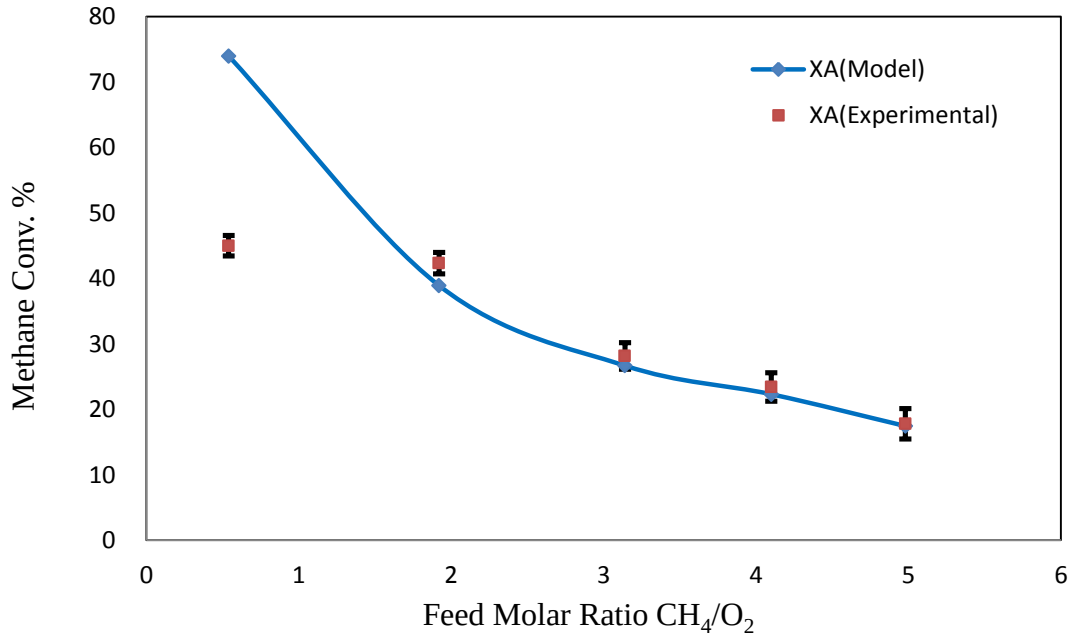

Figure 5.10 Error bar plot for the comparison between model and experiment at 350 ^oC.

The estimated uncertainty in experimental methane conversion X_A increases, on a relative basis, as X_A decreases. However, the model X_A consistently falls within the

uncertainty band of the experimental X_A for nearly every point. The one exception is the point at CH_4/O_2 ratio of 0.54. Since the model does fit the experimental conversion for this feed ratio at other temperatures (e.g. see Figure 5.9), there might be another source of uncertainty regarding this point beyond that of random error.

5.2.3 Arrhenius Plot

The "best fit" k values described in the previous section are presented in Table 5.2.

Table 5.2 Arrhenius Plot Data

k [cm^6/ (min gram mol)]	T (^oC)	T (K)	lnk	1/T
1.60×10^5	250	523	11.9829	0.001912
8.00×10^5	275	548	13.5924	0.001825
7.50×10^6	300	573	15.8304	0.001745
1.10×10^7	325	598	16.2134	0.001672
1.80×10^7	350	623	16.7059	0.001605
2.71×10^7	375	648	17.115	0.001543

Based on the data in Table 5.1, an Arrhenius-type plot is made, shown as Figure 5.12.

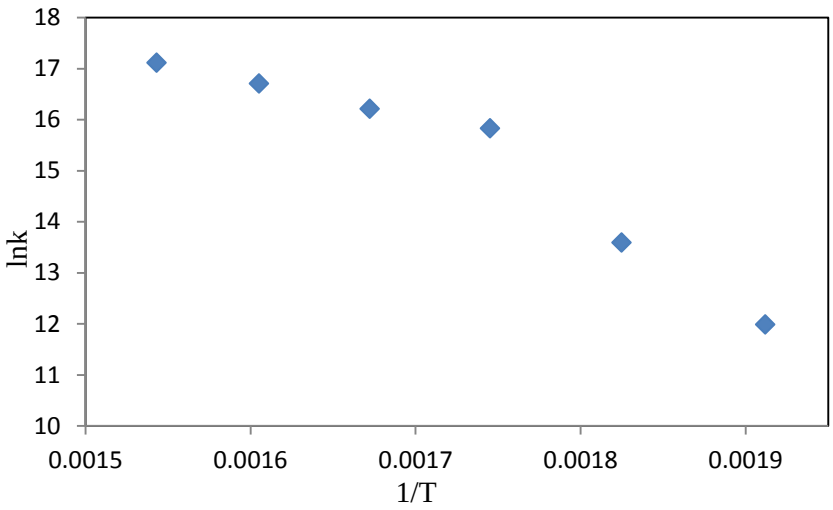

Figure 5.11 Arrhenius plot of "best fit" empirical, global rate constant k.

From Figure 5.11, the relation between ln k and 1/T is linear within the two temperature ranges 250-300 ^{o}C and 300-375 ^{o}C. But the slopes of the two ranges change noticeably at ~300 ^{o}C. This could suggest that the reaction is reaction-limited at lower temperature, changing to mass transfer-limited over 300 ^{o}C. To verify such hypothesis, additional tests, such as new experiments with smaller sized catalyst particles, might reveal in further research. Moreover, diluent other than He would be introduced into new experiments.

5.2.4 Variable Total Flow Rate

A limited number of experiments were run with constant molar ratio of CH_4/O_2, but variable total flow rate. Reaction conditions of these experiments were 50 psig, and molar feed CH_4/O_2=2.0. Reaction temperatures were 300 ^{o}C, 325 ^{o}C, and 375 ^{o}C. The model derived above was then run using the corresponding k values presented in Table 5.1, to see how the model would predict the methane conversions in the variable total flow rate experiments. Comparisons between experimental methane conversions and model

conversions are shown as Figures 5.12-5.14.

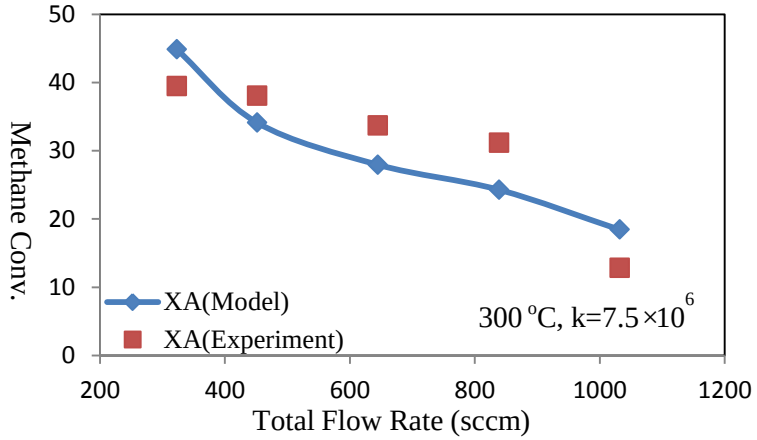

Figure 5.12 Model X_A vs. variable flow rate experimental X_A at 300 °C.

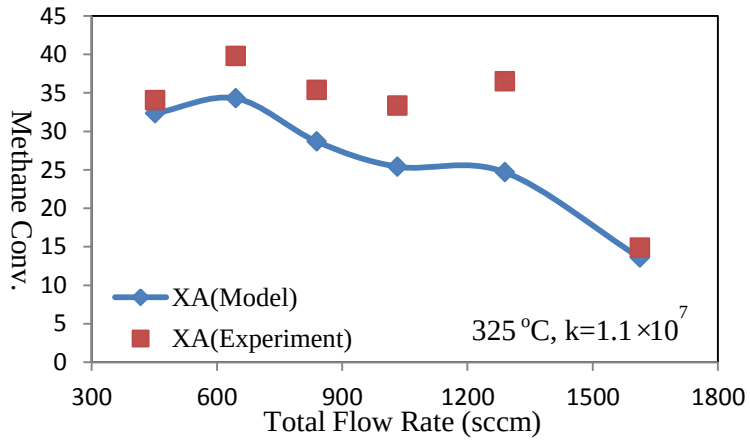

Figure 5.13 Model X_A vs. variable flow rate experimental X_A at 325 °C.

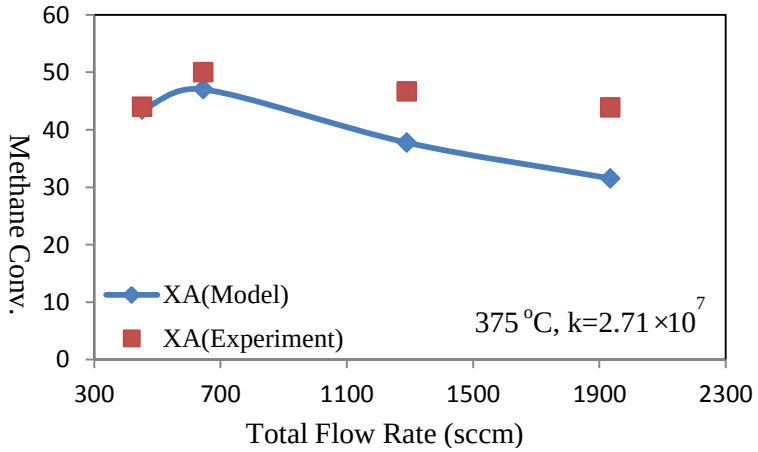

Figure 5.14 Model X_A vs. variable flow rate experimental X_A at 375 °C.

Figures 5.12-5.14 (variable total flow rate for all plots) show us a generally decent-to-good fit between model CH_4 conversion and experimental CH_4 conversion assuming both α and β are 1. Combined with Figures 5.4-5.9, the conclusion can be made that this model (Equation 5.17) shows promise in the prediction of CH_4 conversion in both constant total flow rate experiments and variable flow rate experiments.

$$\frac{dX_A}{dW} = \frac{k}{F_{A0}}\left(\frac{Py_{A0}}{RT}\right)^2 (1 - X_A)\left(\frac{y_{B0}}{by_{A0}} - X_A\right) b \tag{5.24}$$

5.3 Equilibrium Calculation and Result Discussion

5.3.1 Chemical Equilibrium Calculation

A reaction equilibrium calculation is independent of any reaction mechanism or kinetics. It is instructive to compare experimental vs. equilibrium data. In this study, the equilibrium calculations were performed using an on-line resource [19] that uses the STANJAN [20] equilibrium routine. STANJAN provides an efficient algorithm for minimizing the free energy of the mixture to find the equilibrium state. The user specifies the following input information:

- Constraints: e.g. constant T and P (this study), constant H and P
- Starting T and P
- Chemical elements present in the system (He, O, C, H in this study)
- Starting composition
- Chemical species possibly present at equilibrium (He, CO_2, CO, H_2, H_2O, CH_4 in this study)

The equilibrium solver determines the ending composition that minimizes the free

energy of the system, subject to the constraints provided by the user. Figures 5.15-5.17 shows the equilibrium calculating process for a typical case. Reaction conditions were 375℃ and 50psig. Total flow rate was 645 sccm, flow CH_4/O_2 =1.84. Flow rate of He is 590 sccm, feed gas hourly space velocity (GHSV) = 2580 h^{-1}. Figure 5.16 shows the equilibrium calculation results.

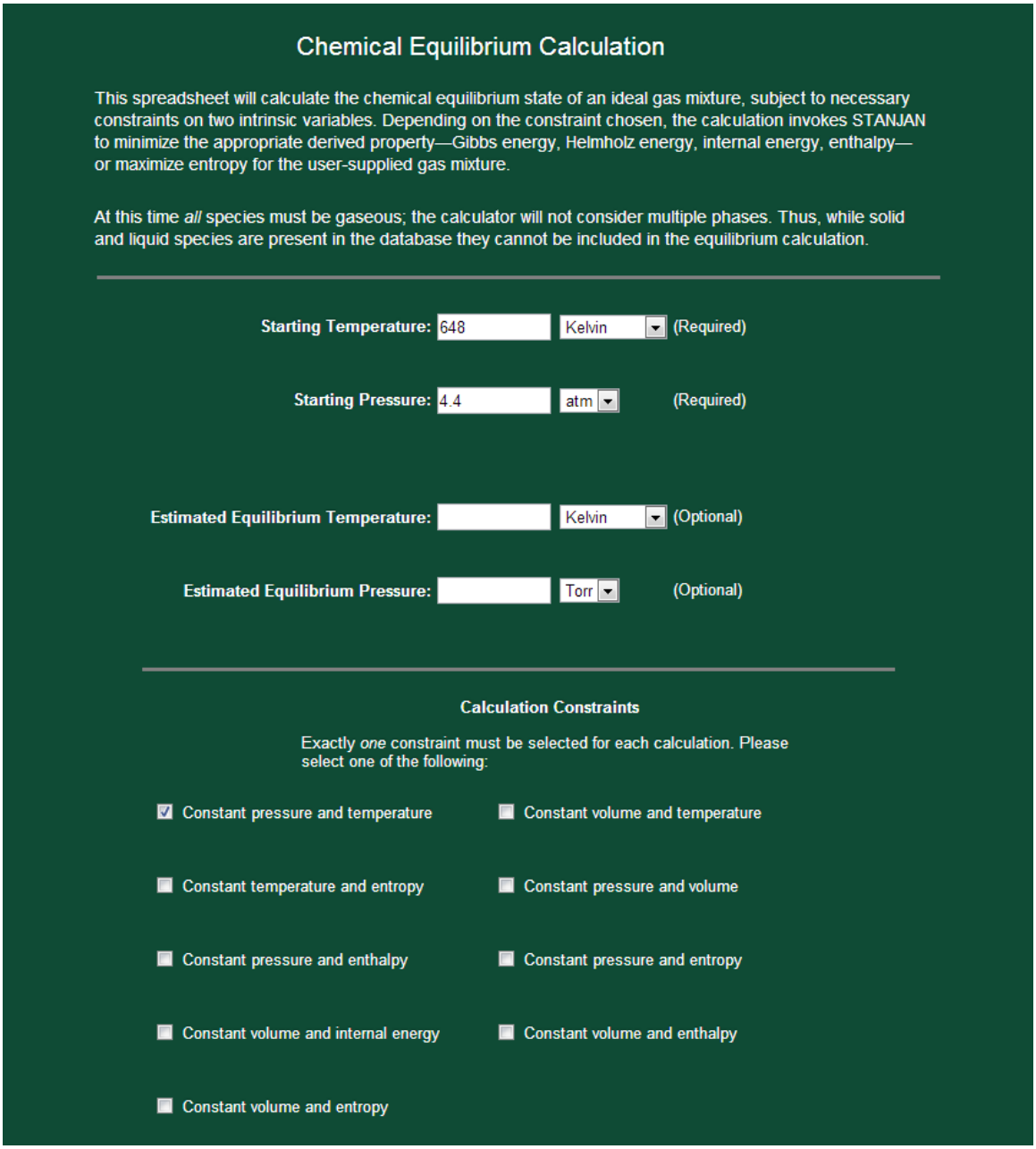

Figure 5.15 Equilibrium calculation of a sample (a).

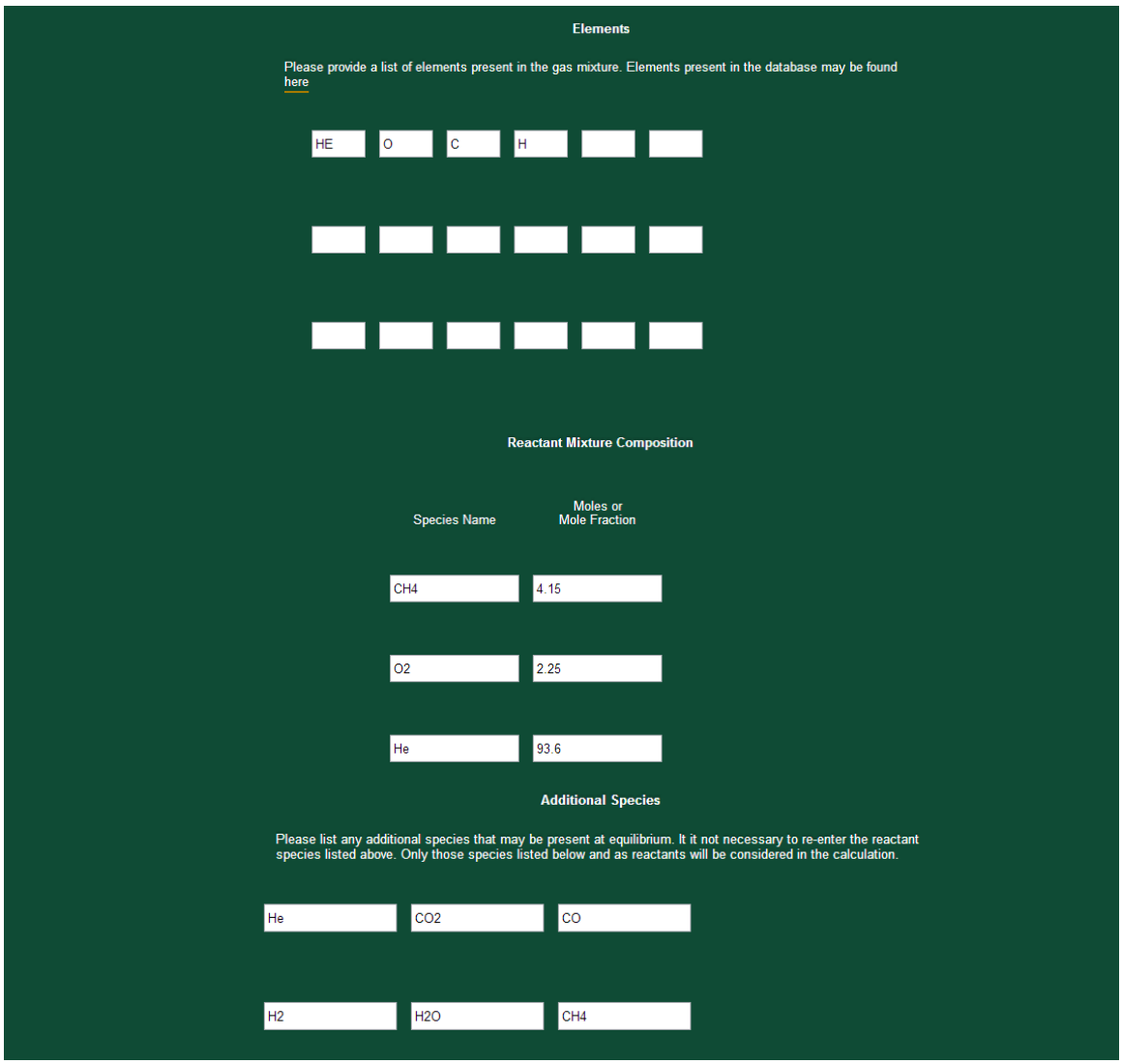

Figure 5.16 Equilibrium calculation of a sample (b).

Chemical Equilibrium Results

	Initial State	Equilibrium State
Pressure (atm)	4.4000E+00	4.4000E+00
Temperature (K)	6.4800E+02	6.4800E+02
Volume (cm^3/g)	2.3547E+03	2.3659E+03
Enthalpy (erg/g)	8.9551E+09	-7.7015E+09
Internal Energy (erg/g)	-1.5429E+09	-1.8249E+10
Entropy (erg/g K)	2.6766E+08	2.6959E+08

	Initial State		Equilibrium State	
	mole fraction	mass fraction	mole fraction	mass fraction
CH4	4.1500E-02	1.2973E-01	2.7711E-02	8.7040E-02
O2	2.2500E-02	1.4029E-01	0.0000E+00	0.0000E+00
HE	9.3600E-01	7.2999E-01	9.3152E-01	7.2999E-01
CO	0.0000E+00	0.0000E+00	4.1767E-04	2.2905E-03
H2	0.0000E+00	0.0000E+00	9.1595E-03	3.6152E-03
H2O	0.0000E+00	0.0000E+00	1.8021E-02	6.3564E-02
CO2	0.0000E+00	0.0000E+00	1.3173E-02	1.1350E-01

Figure 5.17 Equilibrium calculation result.

This equilibrium tool is used for all cases. All results are listed in Appendix Table A.2. Mole fractions of radicals can also be calculated by this solver. Table 5.2 shows common radicals of a typical sample: 375 ℃, 50psig, inlet mole fractions of CH_4, O_2, and He are 0.0173, 0.0323, and 0.9504.

Table 5.3 Common Radicals Mole Fractions

Radicals	Mole Fraction
OH	1.0496×10^{-20}
HO_2	0
H	3.3800×10^{-17}
CH_3	3.5383×10^{-17}

From Table 5.3, mole fractions of these common radicals are all quite tiny. Temperatures are far too low to sustain radicals to any appreciable level. Therefore, data of these radicals are all neglected, neither in Figure 5.16-5.17.

5.3.2 Methane Conversion and Product Selectivity

Methane conversions from equilibrium were also calculated by using Equation 4.2. The results are listed in Appendix Table B.3. Figure 5.18 shows the summery of methane conversions for all temperatures.

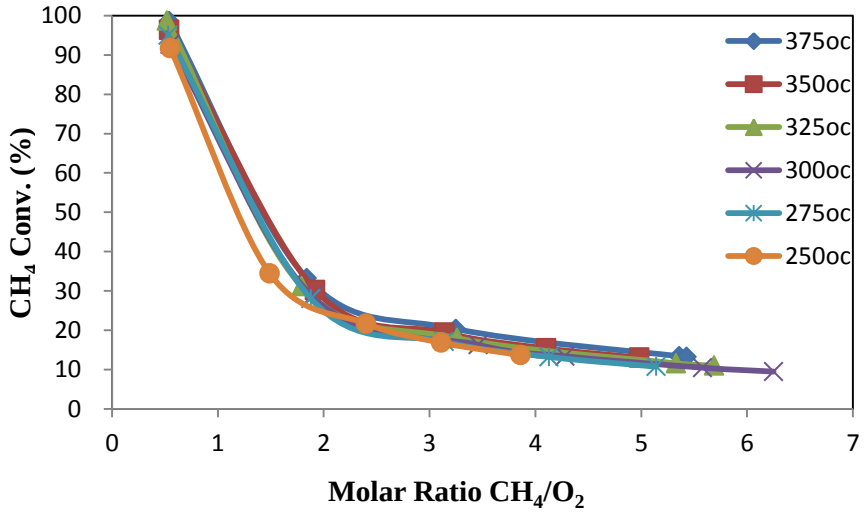

Figure 5.18 Methane conversion for all temperatures from equilibrium calculation.

Figure 5.17 indicates that methane conversions of equilibrium are generally higher than those of catalytic reactions, as highest methane conversion observed is 80.41%. Equilibrium methane conversions are hardly affected by temperature. Compared with Figures 4.1-4.6, the experimental methane conversions of catalytic reactions are more sensitive with the change of temperature.

Product selectivities from equilibrium were also calculated by using Equation 4.4. The results are listed in Appendix Table C.4-Table C.6. Figures 5.19-5.21 show the equilibrium CO selectivity, H_2 selectivity, and CO_2 selectivity.

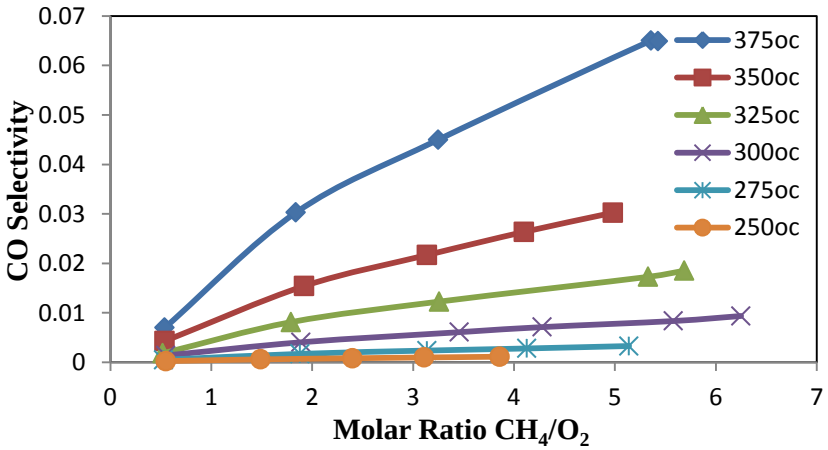

Figure 5.19 CO selectivity vs. feed molar ratio.

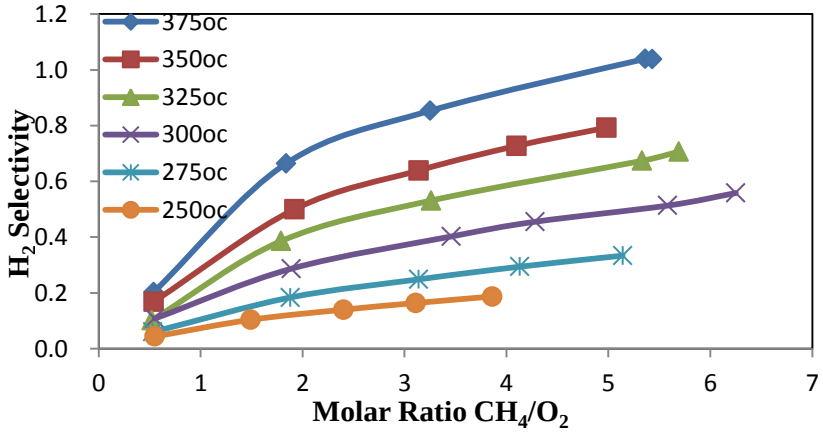

Figure 5.20 H_2 selectivity vs. feed molar ratio.

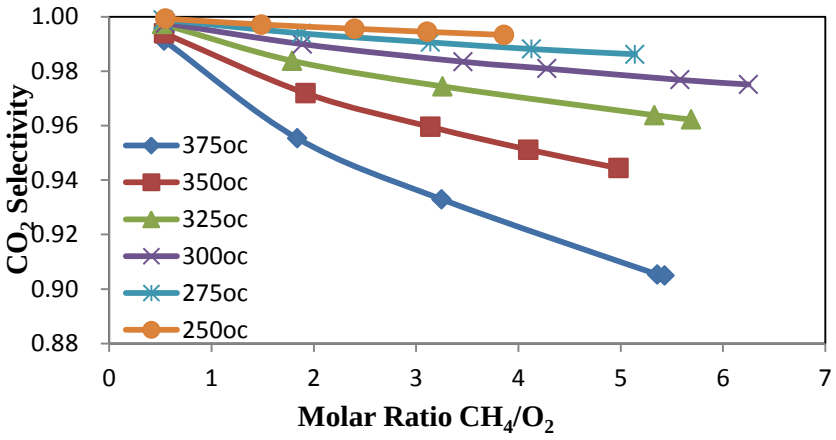

Figure 5.21 CO_2 selectivity vs. feed molar ratio.

Comparing Figures 5.19-5.21 to Figures 4.10-4.12, the equilibrium CO_2 selectivity CO_2 is similar to the experimental CO_2 selectivity. But the equilibrium CO and H_2 selectivities are significantly lower than the experimental values.

The analysis of the comparison between equilibrium calculations and catalytic reactions suggests that the catalyst reaction system is not nearly at equilibrium for CO and H_2. This maybe suggests even more opportunity to improve syngas yields and quality.

CHAPTER 6

CONCLUSIONS

Experiments and modeling have been performed to test the applicability of a heterogeneous phthalocyanine catalyst – specifically, H_{16}PcRu tethered to zeolite catalyst for the partial oxidation of methane into syngas. In this study, 9.91 gram of catalyst was loaded into pecked bed reactor. Experiments were run at 250 ^{o}C, 275 ^{o}C, 300 ^{o}C, 325 ^{o}C, 350 ^{o}C and 375 ^{o}C with a variable feed molar ratio of CH_4/O_2. The catalyst showed impressive activity in converting methane conversions at modest temperatures. The highest methane conversion (80.41%) was observed at 375 ^{o}C and 50psig, with a feed molar ratio CH_4/O_2=0.54, a total flow rate of 645 sccm (91% helium diluent), and a gas hourly space velocity (GHSV) of 2580 hr^{-1}. A 2.96% methane conversion was observed at a reaction temperature is as low as 250 ^{o}C. Compared with 800 ^{o}C, the common process temperature of industrial methane partial oxidation, the phthalocyanine catalyst provides a new option with much lower energy consumption for converting methane into syngas.

Thoroughout the whole study, the H_{16}PcRu-on-zeolite catalyst showed very good activity and stability in the temperature range 250 ^{o}C-375 ^{o}C. Moreover, based on the analysis of the experiment data, excellent carbon balances for all the cases have been observed. This suggests that carbon deposition is very small or negligible.

For methane conversion and product selectivities, which are very important aspects for a potential industrial catalyst, the main influencing factors are reaction temperature and feed molar ratio of CH_4/O_2. From the results of experiments, it is concluded that higher reaction temperature favors higher methane conversion and higher yields of preferred

products distribution; that is high selectivities of CO and H_2, low selectivity of CO_2. Higher molar ratios of CH_4/O_2 also favor production of CO and H_2, but at the expense of methane conversion.

Therefore, based on the available data from this study, the best reaction conditions for this process based on our research is a feed molar ratio CH_4/O_2=2.0 at 375 ^oC with reaction pressure is at 50 psig, total flow rate of 645 sccm, flow rate of He is 590 sccm, and a GHSV of 2580 h^{-1}.

A packed bed reactor species balance was used to model the experiments. Empirical reaction rate constants, as well as global kinetic orders for these rate expressions, were determined from regression of data fitted to this numerical model. Preliminary kinetic analysis indicates a first order dependence on each of methane and oxygen. The global reaction is second-order.

An Arrhenius plot is also made for the global rate constants obtained in this study. The plot shows two obviously different slopes, suggesting that the reaction is reaction-limited in the lower temperature range (250-300^oC), and possibly mass transfer limited in higher temperature range (300-375 ^oC).

Using the derived model and temperature dependent rate constants, methane conversion data from separate variable total flow experiments were reasonably well predicted.

Finally, the catalytic reaction produces CO and H_2 are considerably non-equilibrium levels. This suggests possibly even more room to improve syngas yields and quality.

APPENDIX A

MOLE FRACTION DATA

Table A.1 Mole Fractions of Reactant and Product from Experiment

	Feed CH_4/O_2	Mole Fraction of Feed (%)		Mole Fraction of Outlet (%)					
		CH_4	O_2	CH_4	O_2	CO	H_2	H_2O	CO_2
375 °C	0.54	1.73	3.23	0.34	0.54	0	0	2.46	1.46
	1.84	4.15	2.25	2.08	0.02	0.75	0.99	1.17	1.27
	3.25	4.91	1.51	3.39	0.01	0.61	3.45	0.69	0.85
	5.36	5.36	1.00	4.48	0.01	0.37	3.82	0.49	0.56
	5.43	5.48	1.01	4.65	0.01	0.25	0.47	0.75	0.50
350 °C	0.54	2.12	3.91	1.17	2.18	0	0	1.62	0.92
	1.92	4.93	2.57	2.84	0.01	0.39	2.61	1.51	1.61
	3.14	5.69	1.81	4.09	0	0.42	2.29	0.90	1.15
	4.10	5.95	1.45	4.56	0.01	0.42	2.26	0.70	0.88
	4.98	6.17	1.24	5.07	0.01	0.32	1.73	0.64	0.75
325 °C	0.52	1.69	3.25	0.74	1.37	0	0	1.84	0.96
	1.79	4.10	2.29	2.47	0.01	0.19	1.55	1.51	1.43
	3.26	4.89	1.5	3.97	0.01	0.12	0.11	1.26	0.80
	5.33	5.49	1.03	4.58	0.02	0.19	0	0.39	0.72
	5.69	5.29	0.93	4.52	0.01	0.20	0.98	0.40	0.62
300 °C	0.55	1.78	3.21	0.86	0.48	0	0	1.66	0.90
	1.89	4.16	2.20	2.76	0.01	0.07	0.33	1.69	1.31
	3.46	4.98	1.44	3.94	0.01	0.08	0.61	0.82	0.98
	4.28	5.14	1.2	4.24	0.01	0.08	0.80	0.72	0.79
	5.58	5.69	1.02	5.04	0.02	0.09	1.41	0.61	0.65
	6.25	5.44	0.87	4.8	0.01	0.09	0.80	0.41	0.61
275 °C	0.53	2.02	3.78	1.83	3.35	0	0	0.46	0.20
	1.88	4.79	2.55	4.45	1.95	0	0	0.60	0.30
	3.14	5.65	1.80	5.38	1.27	0	0	0.48	0.29
	4.13	5.94	1.44	5.65	0.83	0	0	0.58	0.32
	5.14	6.22	1.21	5.99	0.78	0	0	0.40	0.23
250 °C	0.55	2.05	3.72	2.00	3.59	0	0	0.16	0.05
	1.49	4.36	2.92	4.28	2.76	0	0	0.16	0.08
	2.40	5.13	2.14	5.05	1.98	0	0	0.14	0.09
	3.11	5.57	1.79	5.46	1.59	0	0	0.18	0.11
	3.86	5.87	1.52	5.76	1.31	0	0	0.20	0.11

Table A.2 Mole Fractions of Reactant and Product from Equilibrium Calculation.

	Feed CH_4/O_2	Mole Fraction of Feed (%)		Mole Fraction of Outlet (%)					
		CH_4	O_2	CH_4	O_2	CO	H_2	H_2O	CO_2
375 °C	0.54	1.73	3.23	0.0252	0	0.0072	0.2834	3.0872	1.6871
	1.84	4.15	2.25	2.7711	0	0.0418	0.9160	1.8021	1.3173
	3.25	4.91	1.51	3.9124	0	0.0226	0.6425	1.1950	0.8962
	5.36	5.36	1.00	4.6428	0	0.0230	0.5705	0.7233	0.6239
	5.43	5.48	1.01	4.7555	0	0.0232	0.5755	0.7308	0.6300
350 °C	0.54	2.12	3.91	0.0764	0	0.0088	0.3446	3.7352	2.0311
	1.92	4.93	2.57	3.4389	0	0.0223	0.7453	2.1990	1.4492
	3.14	5.69	1.81	4.5850	0	0.0240	0.7062	1.4623	1.0603
	4.10	5.95	1.45	5.0345	0	0.0241	0.6658	1.1242	0.8708
	4.98	6.17	1.24	5.3664	0	0.0243	0.6368	0.9297	0.7589
325 °C	0.52	1.69	3.25	0.0218	0	0.0031	0.1697	3.1639	1.6637
	1.79	4.10	2.29	2.8216	0	0.0104	0.4933	2.0428	1.2577
	3.26	4.89	1.5	4.0106	0	0.0108	0.4671	1.2682	0.8569
	5.33	5.49	1.03	4.8543	0	0.0110	0.4282	0.8191	0.6127
	5.69	5.29	0.93	4.7096	0	0.0108	0.4102	0.7284	0.5585
300 °C	0.55	1.78	3.21	0.1297	0	0.0023	0.1784	3.119	1.6464
	1.89	4.16	2.20	2.9680	0	0.0048	0.3420	2.0276	1.18
	3.46	4.98	1.44	4.1700	0	0.0049	0.3260	1.2771	0.7966
	4.28	5.14	1.2	4.4534	0	0.0049	0.3125	1.0443	0.6735
	5.58	5.69	1.02	5.0943	0	0.0050	0.3057	0.8681	0.5819
	6.25	5.44	0.87	4.9245	0	0.0048	0.2877	0.7273	0.5027
275 °C	0.53	2.02	3.78	0.1009	0	0.0010	0.1153	3.7207	1.9170
	1.88	4.79	2.55	3.4485	0	0.0023	0.2464	2.4248	1.3333
	3.14	5.65	1.80	4.6836	0	0.0023	0.2404	1.6788	0.9573
	4.13	5.94	1.44	5.1557	0	0.0022	0.2294	1.3111	0.7680
	5.14	6.22	1.21	5.5524	0	0.0022	0.2228	1.0983	0.6584
250 °C	0.55	2.05	3.72	0.1692	0	0.0005	0.0825	3.6774	1.8795
	1.49	4.36	2.92	2.8586	0	0.0009	0.1557	2.8403	1.4971
	2.40	5.13	2.14	4.0177	0	0.0009	0.1557	2.0609	1.1074
	3.11	5.57	1.79	4.6328	0	0.0009	0.1536	1.7123	0.9320
	3.86	5.87	1.52	5.0684	0	0.0009	0.1500	1.4443	0.7963

APPENDIX B

METHANE CONVERSION DATA

Table B.1 CH_4 Conversion from Experiment and Model with Constant Total Flow Rate

T	Feed CH_4/O_2	X_A from Model (%)	X_A from Experiment (%)
375 °C	5.43	15.30	15.20
	5.36	16.51	16.45
	3.25	30.66	31.06
	1.84	48.10	49.99
	0.54	80.42	80.41
350 °C	0.54	73.98	44.99
	1.92	38.91	42.33
	3.14	26.67	28.13
	4.10	22.30	23.4
	4.98	17.44	17.77
325 °C	5.69	13.57	14.57
	5.33	15.35	16.67
	3.26	18.01	18.73
	1.79	34.28	39.77
	0.52	64.45	56.22
300 °C	6.25	10.76	11.45
	5.58	10.7	11.82
	4.28	15.38	17.34
	3.46	18.07	20.79
	1.89	27.95	33.72
	0.55	56.98	51.53
275 °C	0.53	13.63	9.35
	1.88	7.18	7.13
	3.14	4.86	4.92
	4.13	3.84	4.79
	5.40	3.27	3.74
250 °C	0.55	3.33	2.96
	1.49	2.07	1.87
	2.4	1.52	1.74
	3.11	1.25	1.87
	3.86	1.06	1.98

Table B.2 CH_4 Conversion from Experiment and Model with Variable Total Flow Rate

T	Feed CH_4/O_2	Total Flow Rate (sccm)	X_A from Model (%)	X_A from Experiment (%)
375 °C	1.87	1935	31.53	43.89
	1.89	1290	37.77	46.67
	1.84	645	47.02	49.99
	2.24	452	43.47	43.96
325 °C	1.82	1613	13.58	14.87
	1.92	1290	24.68	36.49
	2.11	1032	25.41	33.35
	2.03	839	28.68	35.36
	1.79	645	34.28	39.77
300 °C	2.12	1032	18.43	12.80
	1.95	839	24.28	31.18
	1.89	645	27.95	33.72
	1.63	452	34.10	38.07
	1.26	323	44.86	39.49

Table B.3 CH_4 Conversion from Equilibrium Calculation

T	Feed CH_4/O_2	X_A from Equilibrium Calculation
375 °C	0.54	98.54
	1.84	33.23
	3.25	20.32
	5.36	13.38
	5.43	13.22
350 °C	0.54	96.40
	1.92	30.25
	3.14	19.42
	4.10	15.39
	4.98	13.02
325 °C	0.52	98.71
	1.79	31.18
	3.26	17.98
	5.33	11.58
	5.69	10.97
300 °C	0.55	92.72
	1.89	28.65
	3.46	16.27
	4.28	13.36
	5.58	10.47
	6.25	9.48
275 °C	0.53	95.00
	1.88	28.01
	3.14	17.10
	4.13	13.20
	5.14	10.73
250 °C	0.55	91.75
	1.49	34.44
	2.40	21.68
	3.11	16.83
	3.86	13.66

APPENDIX C

PRODUCTS SELECTIVITY DATA

Table C.1 Experimental CO Selectivity Data

T	Feed CH_4/O_2	CO Mole Fraction (%)	Reacted CH_4 Mole Fraction (%)	CO Selectivity
375 °C	0.54	0	1.39	0
	1.84	0.75	2.07	0.3623
	3.25	0.61	1.52	0.4013
	5.36	0.37	0.88	0.4205
	5.43	0.25	0.83	0.3012
350 °C	0.54	0	0.95	0
	1.92	0.39	2.09	0.1866
	3.14	0.42	1.60	0.2625
	4.10	0.42	1.39	0.3022
	4.98	0.32	1.10	0.2909
325 °C	0.52	0	0.95	0
	1.79	0.19	1.63	0.1166
	3.26	0.12	0.92	0.1304
	5.33	0.19	0.91	0.2088
	5.69	0.20	0.77	0.2597
300 °C	0.55	0	0.92	0
	1.89	0.07	1.40	0.0500
	3.46	0.08	1.04	0.0769
	4.28	0.08	0.90	0.0889
	5.58	0.09	0.65	0.1385
	6.25	0.09	0.64	0.1406
275 °C	0.53	0	0.19	0
	1.88	0	0.34	0
	3.14	0	0.27	0
	4.13	0	0.29	0
	5.14	0	0.23	0
250 °C	0.55	0	0.05	0
	1.49	0	0.08	0
	2.4	0	0.08	0
	3.11	0	0.11	0
	3.86	0	0.11	0

Table C.2 Experimental H_2 Selectivity Data

T	Feed CH_4/O_2	H_2 Mole Fraction (%)	Reacted CH_4 Mole Fraction (%)	H_2 Selectivity
375 °C	0.54	0	1.39	0
	1.84	0.99	2.07	0.4783
	3.25	3.45	1.52	2.2697
	5.36	3.82	0.88	4.3409
	5.43	0.47	0.83	0.5663
350 °C	0.54	0	0.95	0
	1.92	2.61	2.09	1.2488
	3.14	2.29	1.6	1.4313
	4.10	2.26	1.39	1.6259
	4.98	1.73	1.1	1.5727
325 °C	0.52	0	0.95	0
	1.79	1.43	1.63	0.8773
	3.26	1.55	0.92	1.6848
	5.33	1	0.91	1.0989
	5.69	0.98	0.77	1.2727
300 °C	0.55	0	0.92	0
	1.89	0	0.65	0
	3.46	0.61	1.04	0.5865
	4.28	1.41	0.8	1.7625
	5.58	1.41	0.65	2.1692
	6.25	0.8	0.64	1.2500
275 °C	0.53	0	0.19	0
	1.88	0	0.34	0
	3.14	0	0.27	0
	4.13	0	0.29	0
	5.14	0	0.23	0
250 °C	0.55	0	0.05	0
	1.49	0	0.08	0
	2.4	0	0.08	0
	3.11	0	0.11	0
	3.86	0	0.11	0

Table C.3 Experimental CO_2 Selectivity Data

T	Feed CH_4/O_2	CO_2 Mole Fraction (%)	Reacted CH_4 Mole Fraction (%)	CO_2 Selectivity
375 °C	0.54	1.46	1.39	1.0504
	1.84	1.27	2.07	0.6135
	3.25	0.85	1.52	0.5592
	5.36	0.56	0.88	0.6363
	5.43	0.5	0.83	0.6024
350 °C	0.54	0.92	0.95	0.9684
	1.92	1.61	2.09	0.7703
	3.14	1.15	1.6	0.7188
	4.10	0.88	1.39	0.6331
	4.98	0.75	1.1	0.6818
325 °C	0.52	0.96	0.95	1.0105
	1.79	1.43	1.63	0.8773
	3.26	0.8	0.92	0.8696
	5.33	0.72	0.91	0.7912
	5.69	0.62	0.77	0.8052
300 °C	0.55	0.9	0.92	0.9783
	1.89	1.31	1.4	0.9357
	3.46	0.98	1.04	0.9423
	4.28	0.79	0.9	0.8778
	5.58	0.65	0.65	1.0000
	6.25	0.61	0.64	0.9531
275 °C	0.53	0.2	0.19	1.0526
	1.88	0.3	0.34	0.8824
	3.14	0.29	0.27	1.0741
	4.13	0.32	0.29	1.1034
	5.14	0.23	0.23	1.0000
250 °C	0.55	0.05	0.05	1.0000
	1.49	0.08	0.08	1.0000
	2.4	0.09	0.08	1.1250
	3.11	0.11	0.11	1.0000
	3.86	0.11	0.11	1.0000

Table C.4 Equilibrium Calculated CO Selectivity Data

T	Feed CH_4/O_2	CO Mole Fraction (%)	Reacted CH_4 Mole Fraction (%)	CO Selectivity
375 °C	0.54	0.0119	1.70	0.0070
	1.84	0.0418	1.38	0.0303
	3.25	0.0449	1.00	0.0449
	5.36	0.0467	0.72	0.0649
	5.43	0.0470	0.72	0.0653
350 °C	0.54	0.0088	2.04	0.0043
	1.92	0.0230	1.49	0.0154
	3.14	0.0240	1.11	0.0216
	4.10	0.0241	0.92	0.0262
	4.98	0.0243	0.80	0.0304
325 °C	0.52	0.0031	1.67	0.0019
	1.79	0.0104	1.28	0.0081
	3.26	0.0108	0.88	0.0123
	5.33	0.0110	0.64	0.0172
	5.69	0.0108	0.58	0.0186
300 °C	0.55	0.0023	1.65	0.0014
	1.89	0.0048	1.19	0.0040
	3.46	0.0049	0.81	0.0060
	4.28	0.0049	0.69	0.0071
	5.58	0.0050	0.60	0.0083
	6.25	0.0048	0.52	0.0092
275 °C	0.53	0.0010	1.92	0.0005
	1.88	0.0023	1.34	0.0017
	3.14	0.0023	0.97	0.0024
	4.13	0.0022	0.78	0.0028
	5.14	0.0022	0.67	0.0033
250 °C	0.55	0.0005	1.88	0.0003
	1.49	0.0009	1.50	0.0006
	2.4	0.0009	1.11	0.0008
	3.11	0.0009	0.94	0.0010
	3.86	0.0009	0.80	0.0011

Table C.5 Equilibrium Calculated H_2 Selectivity Data

T	Feed CH_4/O_2	H_2 Mole Fraction (%)	Reacted CH_4 Mole Fraction (%)	H_2 Selectivity
375 °C	0.54	0.3463	1.70	0.2037
	1.84	0.9160	1.38	0.6638
	3.25	0.8509	1.00	0.8509
	5.36	0.7451	0.72	1.0349
	5.43	0.7517	0.72	1.0440
350 °C	0.54	0.3446	2.04	0.1689
	1.92	0.7453	1.49	0.5002
	3.14	0.7062	1.11	0.6362
	4.10	0.6658	0.92	0.7237
	4.98	0.6368	0.80	0.7960
325 °C	0.52	0.1697	1.67	0.1016
	1.79	0.4933	1.28	0.3854
	3.26	0.4671	0.88	0.5308
	5.33	0.4282	0.64	0.6691
	5.69	0.4102	0.58	0.7072
300 °C	0.55	0.1784	1.65	0.1081
	1.89	0.3420	1.19	0.2874
	3.46	0.3260	0.81	0.4025
	4.28	0.3125	0.69	0.4529
	5.58	0.3057	0.60	0.5095
	6.25	0.2877	0.52	0.5533
275 °C	0.53	0.1153	1.92	0.0601
	1.88	0.2464	1.34	0.1839
	3.14	0.2404	0.97	0.2478
	4.13	0.2306	0.78	0.2956
	5.14	0.2228	0.67	0.3325
250 °C	0.55	0.0825	1.88	0.0439
	1.49	0.1557	1.50	0.1038
	2.4	0.1557	1.11	0.1403
	3.11	0.1536	0.94	0.1634
	3.86	0.1500	0.80	0.1875

Table C.5 Equilibrium Calculated CO_2 Selectivity Data

T	Feed CH_4/O_2	CO_2 Mole Fraction (%)	Reacted CH_4 Mole Fraction (%)	CO_2 Selectivity
375 °C	0.54	1.6897	1.70	0.9939
	1.84	1.3173	1.38	0.9546
	3.25	0.9307	1.00	0.9307
	5.36	0.6493	0.72	0.9018
	5.43	0.6556	0.72	0.9106
350 °C	0.54	2.0311	2.04	0.9956
	1.92	1.4492	1.49	0.9726
	3.14	1.0603	1.11	0.9552
	4.10	0.8708	0.92	0.9465
	4.98	0.7589	0.80	0.9486
325 °C	0.52	1.6637	1.67	0.9962
	1.79	1.2577	1.28	0.9826
	3.26	0.8569	0.88	0.9738
	5.33	0.6127	0.64	0.9573
	5.69	0.5585	0.58	0.9629
300 °C	0.55	1.6464	1.65	0.9978
	1.89	1.1800	1.19	0.9916
	3.46	0.7966	0.81	0.9835
	4.28	0.6735	0.69	0.9761
	5.58	0.5819	0.60	0.9698
	6.25	0.5027	0.52	0.9667
275 °C	0.53	1.9170	1.92	0.9984
	1.88	1.3333	1.34	0.9950
	3.14	0.9573	0.97	0.9869
	4.13	0.7750	0.78	0.9936
	5.14	0.6584	0.67	0.9827
250 °C	0.55	1.8795	1.88	0.9997
	1.49	1.4971	1.50	0.9981
	2.4	1.1074	1.11	0.9977
	3.11	0.9320	0.94	0.9915
	3.86	0.7963	0.80	0.9954

APPENDIX D

MODEL ASSEMBLING DATA

Table D.1 Assembling Data for Model Testing

T	Feed CH_4/O_2	Total Flow Rate (sccm)	Fead Flow Rate of CH_4	Fead Flow Rate of O_2	b	y_{A0}	y_{B0}	y_0	Experimental X_A (%)
375 °C	0.54	645	19.29	35.71	1.9353	0.0299	0.0554	-0.001299	80.41
	1.84	645	35.63	19.37	1.0773	0.0552	0.0300	-0.027364	49.99
	3.25	645	42.06	12.94	0.9868	0.0652	0.0201	-0.044879	31.06
	5.36	645	46.35	8.65	1.1250	0.0719	0.0134	-0.05994	16.45
	5.43	645	46.45	8.55	1.2048	0.0720	0.0133	-0.061013	15.2
350 °C	0.54	645	19.29	35.71	1.8211	0.0299	0.0554	0.000495	44.99
	1.92	645	36.16	18.84	1.2249	0.0561	0.0292	-0.03222	42.33
	3.14	645	41.71	13.29	1.1313	0.0647	0.0206	-0.04645	28.13
	4.10	645	44.22	10.78	1.0360	0.0686	0.0167	-0.05243	23.4
	4.98	645	45.8	9.2	1.1182	0.0710	0.0143	-0.05825	17.77
325 °C	0.52	645	18.82	36.18	1.9789	0.0292	0.0561	-0.00083	56.22
	1.79	645	35.29	19.71	1.3988	0.0547	0.0306	-0.03287	39.77
	3.26	645	42.09	12.91	1.6196	0.0653	0.0200	-0.0529	18.73
	5.33	645	46.31	8.69	1.1099	0.0718	0.0135	-0.05966	16.67
	5.69	645	46.78	8.22	1.1948	0.0725	0.0127	-0.06186	14.57

300 °C	0.55	645	19.52	35.48	1.8804	0.0303	0.0550	-0.00101	51.53
	1.89	645	35.97	19.03	1.5643	0.0558	0.0295	-0.03691	33.72
	3.46	645	42.67	12.33	1.3750	0.0662	0.0191	-0.05225	20.79
	4.28	645	44.58	10.42	1.3222	0.0691	0.0162	-0.0569	17.34
	5.58	645	47.41	7.59	1.3438	0.0735	0.0118	-0.06475	11.82
	6.25	645	46.64	8.36	1.5385	0.0723	0.0130	-0.06389	11.45
275 °C	0.53	645	19.05	35.95	2.2632	0.0295	0.0557	-0.00491	9.35
	1.88	645	35.9	19.1	1.7647	0.0557	0.0296	-0.03888	7.13
	3.14	645	41.71	13.29	1.9630	0.0647	0.0206	-0.05417	4.92
	4.13	645	44.28	10.72	2.1034	0.0687	0.0166	-0.06075	4.79
	5.14	645	46.04	8.96	1.8696	0.0714	0.0139	-0.06395	3.74
250 °C	0.55	645	19.52	35.48	2.6000	0.0303	0.0550	-0.00911	2.96
	1.49	645	32.91	22.09	2.0000	0.0510	0.0342	-0.0339	1.87
	2.4	645	38.82	16.18	2.0000	0.0602	0.0251	-0.04764	1.74
	3.11	645	41.62	13.38	1.8182	0.0645	0.0207	-0.05312	1.87
	3.86	645	43.68	11.32	1.9091	0.0677	0.0176	-0.05853	1.98

REFERENCES

1. Alvarez-Galvan, M.C., N. Mota, M. Ojeda, Rojas,S., Navarro, R.M., & Fierro, J.L.G. (2011). Direct Methane Conversion Routes to Chemicals and Fuels. *Catalysis Today*. 171, 15-23.

2. Li,Q. X., Wang,T. F., Liu, Y. F. & Wang, D. Z. (2012). Experimental study and Kinetics Modeling of Partial Oxidation Reactions in Heavily Sooting Laminar Premixed Methane Flames. *Chemical Engineering Journal.* 207-208, 235-244.

3. Jing, Q. S. (2008). *Study of Catalysis Conversion of Methane.* Zheng Zhou University Press. Zhengzhou, Henan Province. (In Chinese)

4. Keller, G.E. & Bhasin, M.M. (1982). Synthesis of Ethylene via Oxidative Coupling of Methane: I. Determination of Active Catalysts. *Journal of Catalysis*. 73 (1), 9-19.

5. Jaso,S., Arellano-Garcia, H, & Wozny, Gunter. (2011). Oxidative coupling of methane in a fluidized bed reactor: Influence of Feeding Policy, Hydrodynamics, and Reactor Geometry. *Chemical Engineering Journal*. 171, 255-271.

6. Gharibi,M., Zangeneh, F. T., Yaripour, F. & Sahebdelfar, S. (2012). Nanocatalysts for Conversion of Natural Gas to Liquid Fuels and Petrochemical Feedstocks. *Applied Catalysis A: General*, 443-444, 8-26.

7. Korup, K., Goldsmith,C. F., Weinberg, G., Geske, M., Kandemir,T., Schlögl,R. & Horn, R. (2013). Catalytic Partial Oxidation of Methane on Platinum Investigated by Spatial Reactor Profiles, Spatially Resolved Spectroscopy, and Microkinetic Modeling. *Journal of Catalysis.* 297, 1-16.

8. Horn,R., Williams, K.A., Degenstein, N.J., Bitsch-Larsen, A., Nogare, D. D., Tupy, S.A. & Schmidt, L.D. (2007). Methane Catalytic Partial Oxidation on Autothermal Rh and Pt Foam Catalysts: Oxidation and Reforming Zones, Transport Effects, and Approach to Thermodynamic Equilibrium. *Journal of Catalysis.* 249, 380-393.

9. Yamagishi,T., Furikado,I., Ito, S., Miyao,T., Naito,S., Tomishige,K. & Kunimori, K. (2006). Catalytic Performance and Characterization of $RhVO_4/SiO_2$ for Hydroformylation and CO hydrogenation. *Journal of Molecular Catalysis A: Chemical.* 244, 201-212.

10. Tomishige, K., Asadullah, M., & Kunimori, K. (2004). Syngas Production by Biomass Gasification Using $Rh/CeO_2/SiO_2$ Catalysts and Fluidized Bed Reactor. *Catalysis Today*, 89, 389-403.

11. Torniainen, P. M., Chu, X., & Schmidt, L. D. (1994). Comparison of Monolith-Supported Metals for the Direct Oxidation of Methane to Syngas. *Journal of Catalysis.* 146, 1-10.

12. Choudhary,V. R., Uphade, B. S. & Mamman, A. S. (1997). Oxidative Conversion of Methane to Syngas over Nickel Supported on Commercial Low Surface Area Porous Catalyst Carriers Precoated with Alkaline and Rare Earth Oxides. *Journal of Catalysis,* 172, 281-293.

13. Choudhary, V.R., Rane,V. H. & Rajput, A. M. (1997). Beneficial Effects of Cobalt Addition to Ni-Catalysts for Oxidative Conversion of Methane to Syngas. *Applied Catalysis A: General,* 162, 235-238.

14. Dissanayake, D., Rosynek, M. P., Kharas, K. C. C. & Lunsford, J. H. (1991). Partial Oxidation of Methane to Carbon Monoxide and Hydrogen over a Ni/Al_2O_3 Catalyst. *Journal of Catalysis.*132, 117-127.

15. Phthalocyanine. *Wikipedia.* Retrieved February 15, 2013, from http://en.wikipedia.org/wiki/Phthalocyanine.

16. Rawling, T & McDonagh, A. (2007). Ruthenium Phthalocyanine and Naphthalocyanine Complexes: Synthesis, Properties and Applications. *Coordination Chemistry Reviews.* 251, 1128-1157.

17. Chan, Y. W., & Wilson, R. B. Jr. (1988) Preprints of Papers -Partial Oxidation of Methane Using Supported Porphyrin and Phthalocyanine Complexes. *American Chemical Society, Division of Fuel Chemistry.* 33, 453-461.

18. Li, C. Q., Manaka, T. & Iwamoto, M. (2003). Static Electric Field Effect in the Second Harmonic Generation from Phthalocyanine Filmymetal Electrode. *Thin Solid Films,* 438- 439, 162-166.

19. http://navier.engr.colostate.edu/~dandy/code/code-4/. Accessed on March 13, 2013.

20. Reynolds. W. C. (1986). "The Element Potential Method for Chemical Equilibrium Analysis: Implementation in the Interactive Program STANJAN". Department of Mechanical Engineering, Stanford University, Stanford, CA, USA.